Title
A TEST OF ISOTOPIC SPIN CONSERVATION IN STRONG INTERACTIONS FROM AN EXPERIMENTAL LIMIT ON cr(d+d-*He4+y)

Author
Pripstein, Morris.

Publication Date
1962-06-01

UCRL 10290

University of California

Ernest O. Lawrence Radiation Laboratory

A TEST OF ISOTOPIC SPIN CONSERVATION IN STRONG INTERACTIONS FROM AN EXPERIMENTAL LIMIT ON $\sigma(d + d \rightarrow He^4 + \pi^0)$

Berkeley, California

DISCLAIMER

Research and Development

UCRL-10290
UC-34 Physics
TID-4500 (17th Ed.)

Abstract

UNIVERSITY OF CALIFORNIA

Lawrence Radiation Laboratory
Berkeley, California

Contract No. W-7405-eng-48

A TEST OF ISOTOPIC SPIN CONSERVATION IN STRONG INTERACTIONS FROM AN EXPERIMENTAL LIMIT ON $\sigma(d + d \rightarrow He^4 + \pi^0)$

Morris Pripstein

(Ph. D. Thesis)

June 1962

Printed in USA. Price $1.75. Available from the
Office of Technical Services
U. S. Department of Commerce
Washington 25, D.C.

A TEST OF ISOTOPIC SPIN CONSERVATION IN STRONG INTERACTIONS FROM AN EXPERIMENTAL LIMIT ON $\sigma(d + d \rightarrow He^4 + \pi^0)$

Contents

Contents (continued)

A TEST OF ISOTOPIC SPIN CONSERVATION IN STRONG INTERACTIONS FROM AN EXPERIMENTAL LIMIT ON $\sigma(d + d \rightarrow He^4 + \pi^0)$

Morris Pripstein

Lawrence Radiation Laboratory
University of California
Berkeley, California

June 1962

ABSTRACT

The reaction $d + d \rightarrow He^4 + \pi^0$, which is forbidden by isotopic spin conservation, has been looked for at the Berkeley 184-inch cyclotron. A beam of deuterons of 460-MeV kinetic energy was scattered from an extended target filled with deuterium gas at a pressure of 390 psi (abs) and at liquid nitrogen temperature. The differential cross section in the center-of-mass system at about $\theta_{c.m.} = 90$ deg was measured and an upper limit of 1.5×10^{-34} cm^2/sr was obtained. The data are consistent with no π^0 production. From a comparison of this upper limit with the theoretical prediction of the cross section for this reaction if isotopic spin need not be conserved, we conclude that isotopic spin is at least 99.6% conserved in strong interactions.

The reaction $d + d \rightarrow He^4 + \gamma$ was also looked for and an upper limit for the differential cross section in the center-of-mass system at $\theta_{c.m.} = 65$ deg of 3.5×10^{-34} cm^2/sr was obtained. The data are consistent with no γ production.

I. INTRODUCTION

In recent years, many experiments have been performed to test the hypothesis of charge independence or isotopic spin conservation in strong interactions.[1] In all cases the experiments tend to confirm the theory, with varying degrees of accuracy, the best of which being the order of 6 to 10%.[1] The method by which these experiments test the conservation law has some inherent limitations which inhibit its sensitivity in verifying the theory. Specifically, the experiments attempt to verify relations between the cross sections of a number of processes predicted by the conservation law by measuring each of the requisite cross sections, with the error in each measurement contributing to the total error of the result; the discrepancy between the experimental and theoretical values of the particular relation investigated is then expressed as the difference of two nearly equal numbers (each of the order of unity), with the result that the discrepancy is dominated by the error in the experimental value which is the percentage error of a large number (unity). To illustrate, consider the following example, which describes one of the more direct tests of the theory in this category.

For the reactions

$$p + d \rightarrow H^3 + \pi^+, \tag{1}$$

and

$$p + d \rightarrow He^3 + \pi^0, \tag{2}$$

the hypothesis of isotopic spin* conservation predicts the relation

$$\frac{\sigma_{H^3}}{\sigma_{He^3}} = 2. \tag{3}$$

---

*Henceforth, isotopic spin is referred to as I-spin.

The Chicago group[2] measured the cross section for Reactions 1 and 2 and found for the ratio

$$\sigma_{H^3}/\sigma_{He^3} = 1.91 \pm 0.25.$$

The possible nonconservation of I-spin is then expressed as the difference between the theoretical and experimental ratios, divided by the theoretical ratio; that is,

$$\text{probability of nonconservation} = 1 - 0.96 \pm 0.13 = (4 \pm 13)\%, \tag{4}$$

so that I-spin conservation is not violated within an accuracy of 13%. From these numbers it is seen that the accuracy of this method of determining possible deviations from the theory is limited by the accuracy with which the various cross sections can be measured. An additional limitation of this method arises from the different charge states of the nuclei and mesons in the reactions to be measured. The resulting electromagnetic perturbation effects cause the ratio of the cross sections as predicted in Eq. (3) to be slightly different than 2. This correction can be calculated to within the experimental accuracy. This type of correction is required in all the experiments that attempt to verify the conservation law by [the method of] measuring relations between cross sections of a number of reactions. The uncertainty in the calculation of this perturbation effect, then, together with the inaccuracy of the measurements, tends to limit the accuracy of this method in verifying the theory.

A more direct and sensitive test of I-spin conservation is to investigate the single reaction

$$d + d \rightarrow He^4 + \pi^0. \tag{5}$$

This reaction, which is a strong interaction, is forbidden by I-spin conservation because it requires a change in I-spin of +1 since the I-spin

of each of the heavy particles is zero whereas that of the ordinary π^0 (member of the charge multiplet π^+, π^0, π^-) is one. Thus, a measurement of the cross section of reaction (5) would indicate directly any possible deviations from I-spin conservation. From this cross section, one can determine, quantitatively, the degree of nonconservation of I-spin by comparing it with the theoretical value of the cross section[3] that was computed under the assumption that I-spin need not be conserved; that is, the ratio of the two cross sections gives an upper limit for the probability of nonconservation of I-spin. Unlike the method described above, this method is not particularly sensitive to the experimental accuracy, since the error on the limit of nonconservation expressed in this way is the percentage error of a very small number. To illustrate this point, suppose that the ratio of the experimental to the theoretical cross section is 10^{-2} and that the error in the measurement of the experimental cross section is 50%. Then,

$$\text{the probability of nonconservation of I-spin} = 0.01 \pm 0.50 \times 0.01 = (1.0 \pm 0.5)\%. \tag{6}$$

Thus, the effect of the large experimental error in this case is not as significant as in the method described above in determining the possible violation of the conservation law by this method.

Then, to test the validity of the hypothesis of I-spin conservation by a direct method, an experiment was performed at the Berkeley 184-inch cyclotron to investigate Reaction (5). With the same setup, the reaction

$$d + d \rightarrow He^4 + \gamma \tag{7}$$

was also looked for.

II. EXPERIMENTAL METHOD

A. General Description

We studied the π^0 reaction (Reaction 5) by looking for α-particles produced from a gas deuterium target bombarded by a beam of deuterons of 460 MeV kinetic energy (lab) from the Berkeley 184-inch cyclotron. The design of the experimental setup was determined by the following factors:

(a) The π^0 reaction if it exists, has a very small cross section; previous investigations of this reaction have obtained upper limits for the total cross section of 7×10^{-32} cm^2 at 460 MeV,[4] and 2×10^{-32} cm^2 at 400 MeV.[5] Since these are only upper limits, the experiment must be designed to measure a cross section much smaller than these limits.

(b) The kinematics of the π^0 reaction, $d + d \rightarrow He^4 + \pi^0$, and the γ reaction,

$$d + d \rightarrow He^4 + \gamma .$$

(c) Space and magnet-power limitations at the 184-inch cyclotron.

In the measurement of such a small cross section the problem of background becomes very important. Since the π^0 reaction is to be identified by the detection of α-particles from the deuterium target, the major source of background is the production of α-particles in the portion of the walls of the target situated directly in the path of the deuterium beam. This background can be eliminated by using an extended target and detecting α-particles that come off at some lab angle, θ with respect to the incident deuteron beam direction. A collimator can then be built along the θ direction that will not "see" the portion of the target walls hit by the intense deuteron beam; that is, any α-particle produced at the walls of the target by the primary deuteron beam cannot get through the alpha-beam collimator. This is illustrated in Fig. 1.

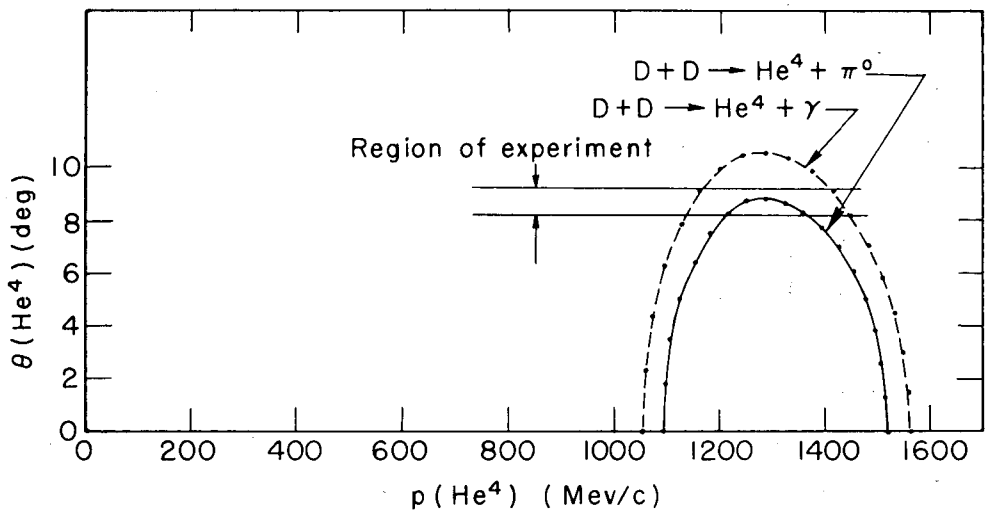

MU-22451

Fig. 2. Angle vs. momentum of He^4 in the lab. Points are plotted in 10-deg intervals of center-of-mass angle.

If $\Delta\theta_{lab}$ were made larger than ± 0.6 deg to increase the solid angle for the π^0 reaction, the momentum bite of the magnet system would have to be correspondingly larger to accept the additional α-particles; then α-particles from the γ reaction would also be accepted by the system.

To optimize the search for the π^0 reaction, then an extended high-pressure deuterium-gas target cooled to liquid nitrogen temperature was built; also, a magnet system was designed which selected positive charged particles of a certain effective momentum p/z, and within a momentum bite of $\pm$ 6%, coming off the target at a lab angle of 8.7 ± 0.6 deg, and which delivered them outside the main shielding of the physics cave into a blockhouse of relatively low background. A collimator, consisting of two lead slits, was placed at the entrance of the magnet system to define the direction of the secondary beam and to exclude background from the walls of the target. A system of counters separated α-particles from the other components in this secondary beam. The experimental arrangement is shown in Fig. 3 and details are given in Table I. To minimize energy loss and multiple scattering, the α-particle beam is passed entirely through a vacuum, except for regions near the target and in the vicinity of the counters.

To measure sources of background, data runs were also taken with hydrogen gas in the target. No alphas can come from d-p collisions (conservation of baryons) and since any charged particle suffers the same dE/dx in the hydrogen and deuterium gas (at the same pressure and temperature), the hydrogen data were treated as background and subtracted from the deuterium data to yield the net He^4 signal from the d-d collisions. However, this signal is to be considered as an upper limit because a D_2-H_2 subtraction of the data does not cancel the effect of all sources of background. This point is discussed more fully in Sec. IV-C.

The γ reaction, (7), was also looked for at $\Theta_{c.m.} = 65$ deg by setting the magnet system for momentum 1427 MeV/c and taking data runs with deuterium and hydrogen gas in the target. To gain additional information about background, the low-momentum side of the γ reaction, at $\Theta_{c.m.} = 135$ deg, was also investigated by setting the magnet system for momentum 1150 MeV/c.

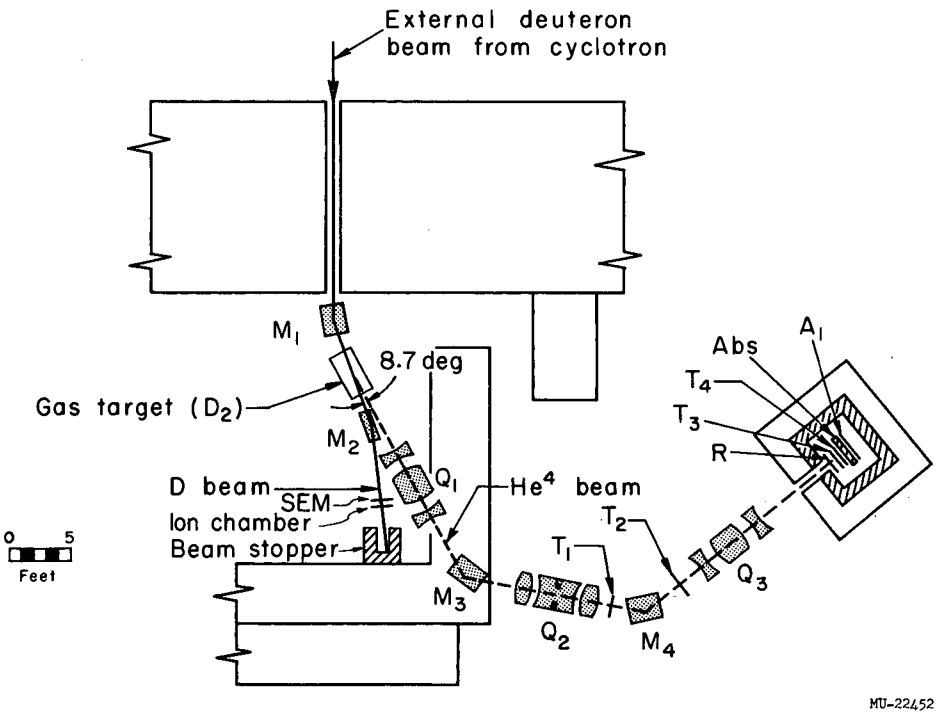

Fig. 3. Plan view of physics cave and arrangement of experimental apparatus.

Table I. Magnet system and counter telescope components shown in Fig. 3.

Item	Designated symbol	Description
Bending magnets	M_1	Low-powered H magnet with 7-in. gap, 29×36-in. rectangular pole tips, 21 deg bend.
	M_2	High-powered C magnet with 3.5-in. gap, 6×26-in. rectangular pole tips, 15-deg bend.
	M_3, M_4	High-powered H magnet with 8-in. gap, 18×36-in. rectangular pole tips, 50-deg bend.
Strong-focusing Magnetic quadrupoles	Q_1, Q_3	8-in-aperture, three-element (16-32-16-in.) quadrupole focusing magnet, operated DCD(divergent-convergent-divergent)in horizontal plane.
	Q_2	8-in. aperture, three-element (16-32-16-in.) quadrupole focusing magnet, operated CDC (convergent-divergent-convergent) in horizontal plane.
Counter telescope	T_1, T_2	Plastic scintillator, 6.5×6.5×0.020 in., located 261 in. and 190 in., respectively, upstream from final image position.
	T_3, T_4	Plastic scintillator, 4×4×0.020 in., located at final image position.
	R	Plastic scintillator, 4×4×0.063 in., located 8 in. upstream from final image.
	Absorber	CH_2, located 5 in. downstream from final image.
	A_1	Plastic scintillator, 6.5×6.5×0.020 in. located 12 in. downstream from final image.

B. Deuteron Beam

The requirements for the external 460-MeV deuteron beam were that it be parallel in the horizontal plane at the D_2 target and small in cross-sectional size. More specifically, the beam had to be sufficiently narrow in the horizontal plane so that the difference in α-particle path length in deuterium between alphas produced at either boundary of the deuteron beam was small--small enough for the momentum difference of these alphas at the target exit due to their variation in energy loss as a result of their path difference to be smaller than the momentum bite of the alpha-selecting magnet system. With reference to Fig. 4, this condition may be stated as follows: The difference in α-particle path length in deuterium, MN, must be sufficiently small so that alphas of the same momentum produced at points M, Y, and N have a $\Delta P/P$ at the target exit (point 3), which is smaller than the $\Delta P/P$ of the alpha-selecting magnet system. An additional requirement is that the position and the direction of the deuteron beam at the target must be accurately determined.

A plan view of the Berkeley 184-inch synchrocyclotron and the regenerated-deuteron-beam orbit is shown in Fig. 5. The beam was collimated at the entrance of the steering magnet and focused by an 8-in.-aperture two-element strong-focusing quadrupole magnet to provide a spot 1/2 in. wide and 1.5 in. high at the D_2 target. This was the smallest beam spot that could be achieved with no appreciable loss of beam intensity. The parallel condition of the beam was checked by exposing x-ray films placed along the deuteron beam line between the physics cave snout and the D_2 target. The exposures indicated that there were no intermediate optical image points between the focusing quadrupole and the D_2 target. Since the bending magnet, M_1, provides no focusing action in the horizontal plane, the angular spread of the deuteron beam at the target is determined from the width of the beam at the quadrupole and at the target, and from the distance between these

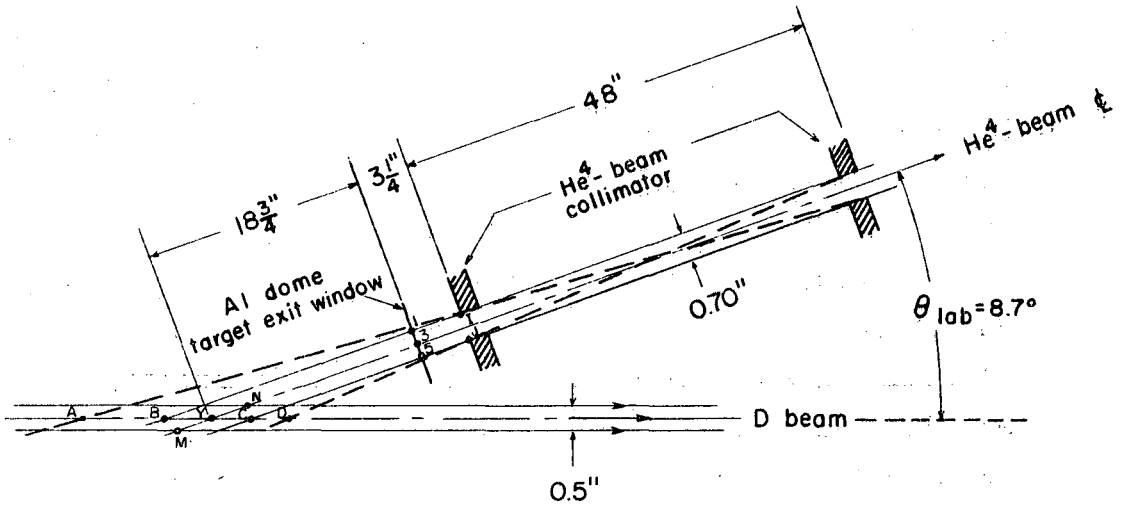

Fig. 4. Configuration of deuteron and alpha beams at D_2 target (horizontal plane).

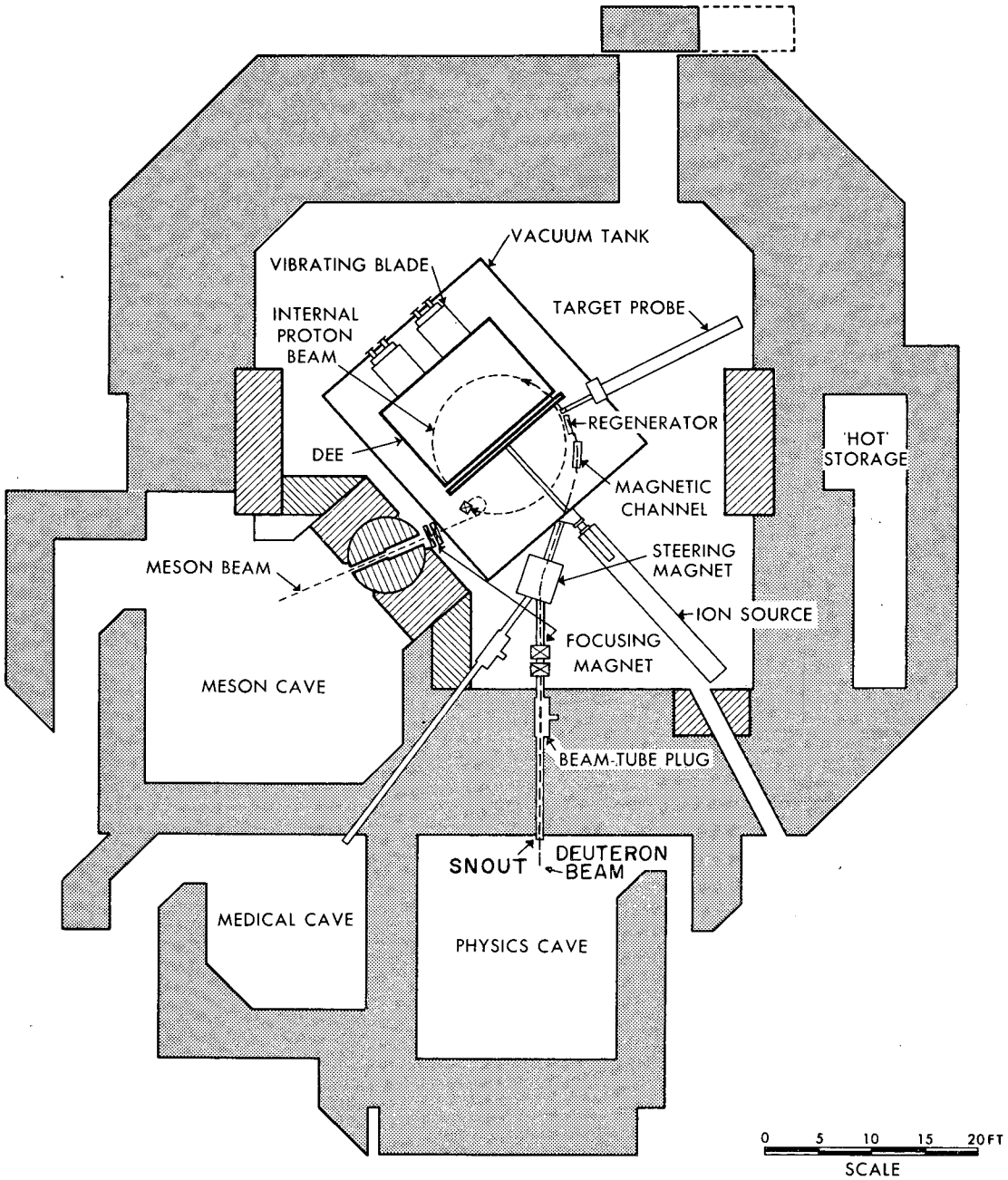

Fig. 5. Plan view of deuteron orbit from 184-inch synchro-cyclotron.

two points. From x-ray film exposures at the quadrupole, taken before the experiment,[8] the width of the beam at this magnet was determined to be 2/3 in. in the horizontal plane. Since the target was located 300 in. downstream from the quadrupole, the angular spread of deuteron beam at the target was smaller than ± 0.14 deg in the horizontal plane. As this was much smaller than the $\Delta\theta$ subtended by the secondary alpha-beam collimator, the parallelism requirement of the deuteron beam was satisfied.

For the beam spot size and the amount of deuterium in the target described, alphas produced with the same momentum at points M, Y, N (Fig. 4) had, at the target exit, a momentum difference between them of $\Delta P/P = 1.3\%$. Since the momentum bite of the magnet system was approximately ± 6%, the requirements for the deuteron beam were achieved. The position and direction of the deuteron beam were checked periodically by exposing x-ray film at the entrance and exit windows of the target. The primary collimation of the deuteron beam was done upstream of the steering magnet rather than in the snout of the beam pipe at the entrance to the physics cave, in order to decrease the background in the cave.

At the entrance of the physics cave, the deuteron beam was deflected 21 deg by bending magnet M_1, described in Table I, toward the D_2 target. Bending the beam before the target allows the magnet system to be conveniently located with respect to the shielding of the cave and the walls of the cyclotron building, and sweeps out any low-energy charged-particle background coming from the walls of the snout. Collimation of this background was provided by 2-in. -wide lead slits placed at the beam-pipe snout and at the target entrance.

After the deuteron beam passed through the target, it was bent 15 deg away from the alpha beam side into a beam stopper by means of the C magnet M_2. This permitted quadrupole Q_1 to be closer to the D_2 target in order to increase the solid angle of the alpha-selecting magnet system. Since the alpha beam passes near the pole tips of M_2, it was necessary to shield the alpha beam from the fringe field of M_2.

A thick magnetic shield made of cold-rolled iron piping was built and attached to the side of M_2. Details are shown in Fig. 6. Mylar windows 0.006 in. thick were put on the ends of the shield so that a vacuum (a few microns pressure) would be maintained inside the shield.

C. Deuteron-Beam Monitor

The deuteron beam incident on the D_2 target was monitored by a secondary-emission chamber (SEM). The SEM used is identical to the one described by Larsen.[9] During the experiment, the SEM was 5 ft. downstream from the exit of M_2. We centered it on the deuteron beam line by exposing x-ray film in front of and behind it. The SEM was calibrated against an argon-filled ionization chamber (Fig. 7) placed next to the exit face of the SEM. The ion chamber had a sensitive area equal to that of the SEM. With the SEM set at a reasonable voltage (1000 v), a voltage plateau of the ion chamber was made by measuring the current from the ion chamber per unit current from the SEM as a function of the ion chamber voltage. The voltage was then set at a value on the plateau (Fig. 8). These measurements were performed at a very low beam intensity, at which the response of the ion chamber was linear. We then measured voltage plateau of the SEM by using the ion chamber as a monitor (Fig. 8). The resulting voltage plateau illustrates a useful feature characteristic of a SEM operated in a magnetic field-free region: the output current is independent of collecting voltage over a wide range of voltage. This is a result of the preponderance of low-energy electrons, which are easily collected.

An intensity plateau of the ion chamber was measured with the SEM as a monitor, since the SEM output is linear as a function of beam intensity. With the beam intensity held at a particular level, we measured the integrated current collected by each chamber by passing it into a condenser and measuring the potential across the condenser with an electrometer circuit. The output of the electrometer was displayed on a recorder. This measurement was repeated for beam levels between maximum beam and 0.2% of the maximum.

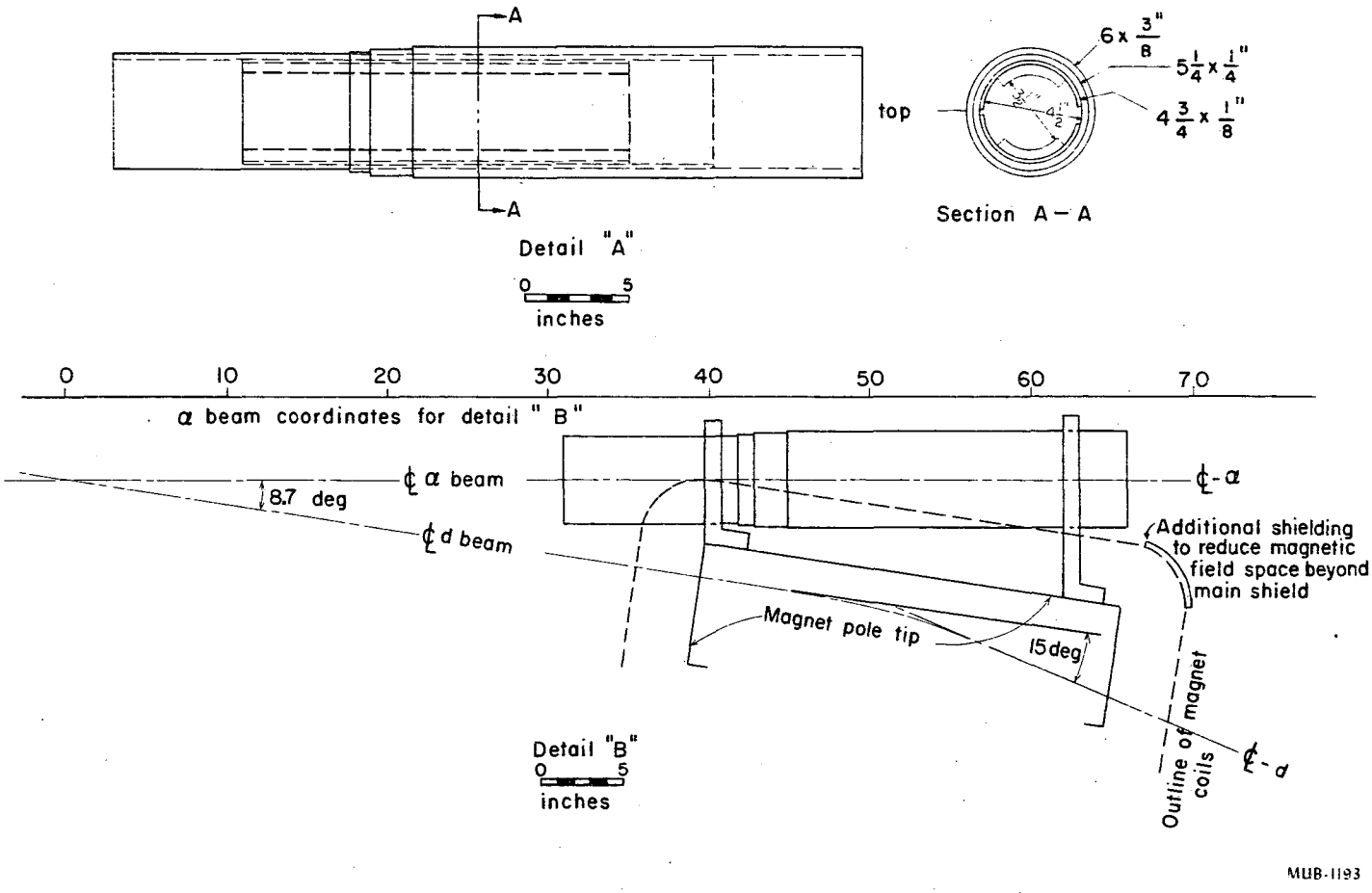

Fig. 6. C-Magnet (M_2) fringe field shield. A. Detail of shield. B. Detail of shield mounting. Schematic diagram of argon-filled ion chamber.

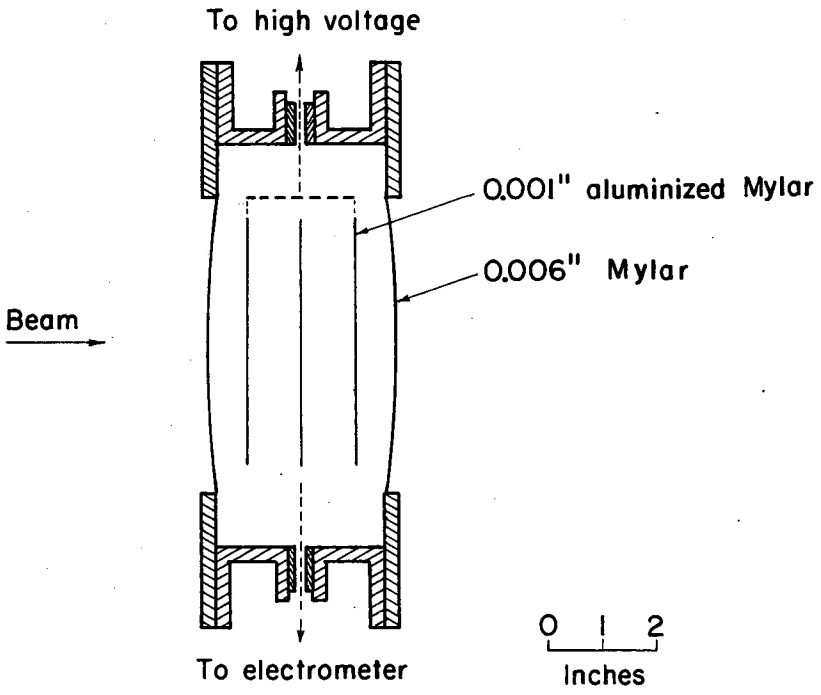

Fig. 7. Argon temperature = 25°C; argon pressure = 17.2 psi (absolute).

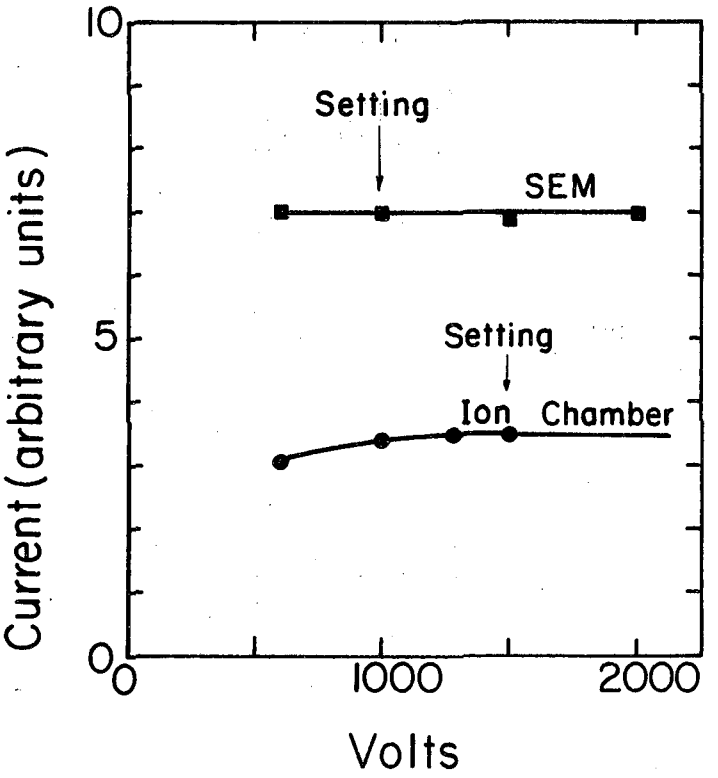

Fig. 8. Voltage plateaus of beam monitors. The data for a particular chamber have been arbitrarily normalized since the slopes are the significant information.

During the calibration run, the drift current, which is the current from the chamber with the beam off, was measured and found negligible. The reproducibility of the SEM was checked and found to be within 1.3%.

To measure the amount of beam that did not pass through the SEM in its normal position because of multiple scattering in the target, the SEM current per unit ion-chamber current was measured for the SEM in its normal position and at the target exit, with the ion chamber remaining in its normal position. From these two numbers, the amount of beam that passed through the D_2 target but did not enter the SEM in its normal position was 6%. Since the thickness of the SEM was much less than that of the target, the presence of the SEM near the target did not change the number of deuterons passing through the ion chamber. With the foregoing data, the deuteron beam intensity into the target per μA of SEM current was calculated to be $0.67 \pm 0.01 \times 10^{13}$ particles/sec. The calculation is included in Appendix A. The error on this number is the measure of the reproducibility of the SEM and of the accuracy with which the temperature and pressure of the ion chamber could be determined. The normal beam intensity used during the experiment was about 1.7×10^{10} deuterons/sec.

D. Alpha-Beam System

1. General Features

The magnet system was designed to be achromatic for a momentum bite of approximately $\pm 6\%$. The layout of the system is shown in Fig. 3 and a description of the component magnets is included in Table I. The optics for the system are shown schematically in Fig. 9. Except for the presence of the two very thin time-of-flight counters, T_1 and T_2, the beam was perfectly symmetric about the center of the field lens Q_2. Thus, Q_3 and M_4 were operated identically to Q_1 and M_3, respectively.

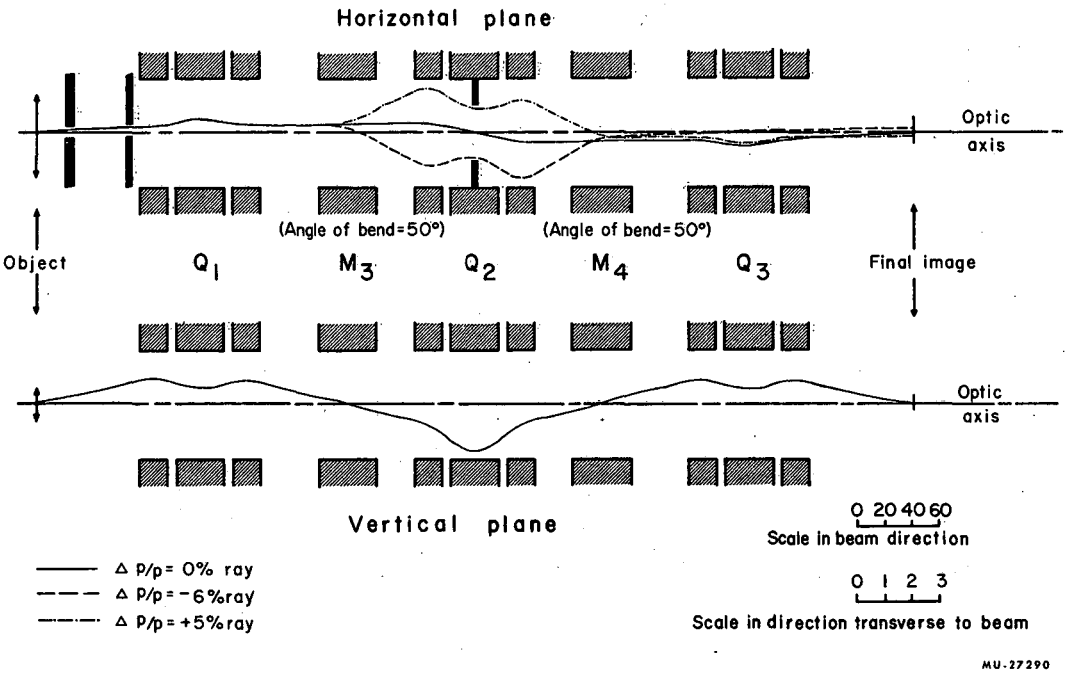

Fig. 9. Beam optics.

The final image in the system was at counters T_3, T_4, and A_1, which were located in a blockhouse whose walls consisted of a layer of 1-ft-thick steel inside a layer of 2-ft-thick paraffin. The background in this confined area was negligible. A lead collimator was placed between the target and Q_1 to fix the lab angle of the α-particles at 8.7 ± 0.6 deg and to prevent the magnet system from seeing the deuteron beam as it passed through the windows of the target. The collimator consisted of two lead slits, each 0.70 in. wide, with the upstream slit located 22 in. away from the target center, and the second slit at the entrance of Q_1, 70 in. away from the target center.

To minimize energy loss and multiple scattering, the α-particle beam is passed entirely through a vacuum except for regions near the target and the counters. The vacuum system consisted of 0.25-in-thick, 7-in. -i. d. aluminum pipes in the quadrupoles and a 0.5-in. -thick aluminum box, 17 in. wide × 35 in. long × 7 in. high, in the gap of M_3 and M_4.

The large angle of bend in M_3 and M_4, 50 deg, was necessary so that the experimental setup would be conveniently positioned with respect to the shielding walls of the physics cave and the exterior walls of the cyclotron building. An advantage of having a large bend is that it reduces the background at the final counters; however, a bend of 50 deg causes sufficiently large dispersion in M_3 and M_4 to reduce the phase space of the magnet system for the extreme momenta $\Delta P/P = \pm 6\%$. Were it not for the space limitation at the 184-inch cyclotron, an angle of bend of about 38 deg would have been preferable, as it would have given a larger magnet-system phase space.

2. Beam Optics in Horizontal Plane

In this plane, Q_1 was operated to image the target onto the center of Q_2. Since the width of the alpha beam was narrow because of the collimator in front of Q_1, only a small part of the effective horizontal aperture of Q_1 was illuminated with α-particles; consequently, Q_1 was operated with DCD polarity (Divergent-Convergent-Divergent) in this plane, and therefore CDC in the vertical plane. If the polarity

of Q_1 were reversed, the effective aperture in the vertical plane would be decreased although the aperture in the horizontal plane would still be determined by the collimator, so that the solid angle subtended at the target by Q_1 and the slit system would be reduced.

The bending magnet M_3 was oriented so that the angles between the beam center line and the entrance and exit faces of M_3 were equal. Under these conditions, M_3 provided no focusing action in the horizontal plane.

The purpose of the field lens Q_2, was to recombine the different particle momenta dispersed by M_3. This recombination was accomplished by having Q_2 image the center of M_3 (i.e., the center of the dispersion) onto the center of M_4. Because of the large dispersion in the bending magnets, Q_2 was operated with CDC polarity in the horizontal plane.

To define the momentum bite of the system, a brass slit, 4 in. wide, was placed at the center of Q_2, the point of symmetry in the system; this point is the first image position of the target for the central momentum rays in the horizontal plane. The slits were placed here to provide a sharply defined (nearly rectangular) momentum spectrum.[10] The final image of the system in both planes was formed at the last counters, which were at a distance from Q_3 equal to that of the target from Q_1.

The salient feature of the horizontal-plane optics for a system operated in this way was that the energy focus of the system coincided with the horizontal focus[10,11,12] (i.e., the focus in the horizontal plane for central momentum particles). This condition minimizes final horizontal image size. A complete analysis of this feature is given by K. L. Brown.[10]

3. Beam Optics in Vertical Plane

We determined the optics in this plane primarily from solid-angle considerations. As in the horizontal plane, the optics of the system are symmetric about the center of Q_2. Ordinarily, for a system of this type, Q_1 should be operated in such a way that the combined effect of Q_1 and M_3 would be to image the target onto the entrance

principal plane of Q_2, making the optics in the vertical plane independent of the operating conditions of the field lens. For purposes of optical brightness, the field lens Q_2 should image the exit principal plane of Q_1 onto the entrance principal plane of Q_3.

The optics of our system deviated from the preceding conditions in order to increase the phase space of the magnet system.* Because of the large angle of bend in M_3 (and M_4), M_3 acts like a very strong converging lens (short positive focal length); thus for the target to be imaged onto the Q_2 principal plane, Q_1 would have to be diverging in the vertical plane. As a result, the first optical stop would occur at M_3. To make the first optical stop occur in Q_1, with a resultant increase in solid angle, we operated Q_1 as a converging lens to image the target onto the center of M_3. The field lens, Q_2, was then operated to image the center of M_3 onto the center of M_4. The optical properties of Q_3 were the same as those of Q_1.

---

*The concept of phase space to describe the transmission of a magnet system is discussed more fully by Devlin.[13] Briefly, if a coordinate system is defined with its origin at the source of particles (i.e., at the target) and the z-axis along the direction of the central ray, then we can consider two phase spaces, namely, in the horizontal and vertical planes (zx and zy planes). The position of a particle in phase space is given by its displacement (x or y) from the central ray in the horizontal or vertical plane, and by its slope (dx/dz or dy/dz) with respect to the central ray in that plane. The phase space of the magnet system is then the four-dimensional volume $\int\int\int\int dx\, dy\, d(dx/dz)\, d(dy/dz)$ subtended at the target by the limiting optical stops propagated back through the system to the target. The number of particles transmitted by the magnet system is then proportional to this volume in phase space.

4. Transmission of Magnet System and Beam Tune-Up.

The currents and focusing properties for the bending magnets were carefully determined by the wire-orbit method. The currents in the quadrupoles were determined before the experiment by an IBM 650 computer program (Tripole).[14] For a particular momentum, a given position of the object, and a desired position of the image with respect to the quadrupole, the Tripole program calculated the necessary magnetic-field gradient (hence, the current) for each element of the lens. The predicted current values from Tripole were checked experimentally by the wire-orbit method. The matrices which describe the focusing action of bending magnets M_3 and M_4 were obtained from Cross's equations[15] and from Penner.[12] The effective length of each magnet was determined from the wire-orbit data. The validity of Cross's equations was checked by comparing the focusing properties of M_3 and M_4, as calculated by these equations, with the wire-orbit data. The discrepancy between the calculated and measured values was less than 10%.

The transmission of the magnet system as a function of $\Delta P/P$ was determined analytically by tracing a large number of rays through the system by means of matrix equations. Each quadrupole element was subdivided into four parts, with each part described by the appropriate matrix.[16,17] More than 100 rays of different momenta, coming from all parts of the target and at various angles, were traced through the magnet system by means of a matrix multiplication computer program. This was done for both the horizontal and vertical planes. From these ray traces, the size of the momentum-defining slits needed at the center of Q_2 was determined to be 4 in. wide. A graph of the transmission versus $\Delta P/P$ for the resulting system is shown in Fig. 10, with the transmission for the central momentum normalized to unity. Transmission in this context is defined as the ratio of the number of rays from the target that are transmitted through the whole magnet system into the final counters to the number of rays from the target that are accepted by the collimator. The transmission, then, is directly proportional to the magnet-system phase space. The spectrum

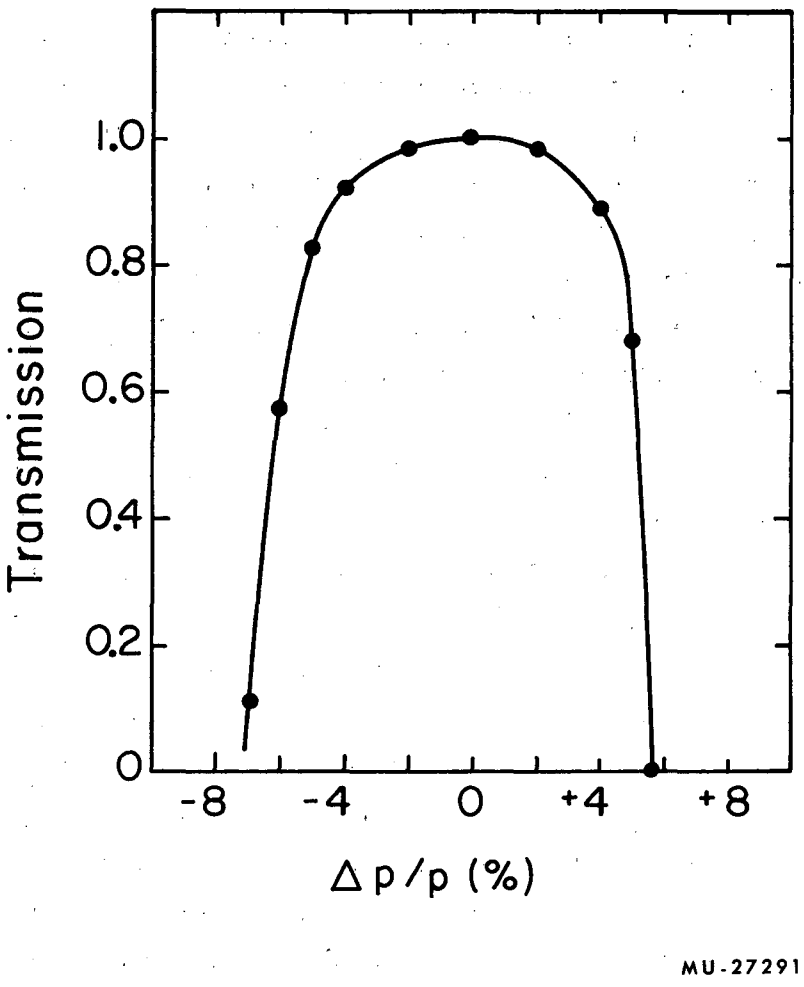

Fig. 10. Momentum spectrum transmitted by the magnet system (calculated).

is not symmetric about the central momentum because of the chromatic aberration of the quadrupoles. The width and shape of the transmission curve were limited by the size of the momentum-defining slits and the dispersion in M_3 and M_4. For a smaller angle of bend in M_3 and M_4, the shape of the momentum spectrum would be more nearly rectangular.

From the ray trace, the effective vertical aperture at the entrance of Q_1 was determined to be 3.1 in. Thus, the total effective aperture at the entrance of Q_1 (70 in. from the target center) is 0.70 in. $\times$ 3.10 in. The size of the final image was also obtained from the ray trace. Since this is a quantity which can be easily measured experimentally, the final image sizes for various collimators in front of Q_1 were also calculated. A comparison of the calculated values with those obtained experimentally for the corresponding collimator configuration would indicate the validity of the calculated momentum spectrum for the system. (For this particular magnet system, the only place that the properties of the beam can be properly studied is at the final image position; therefore, the most accurate information about the beam will be derived from the profiles at this point).

The beam tune-up was accomplished by scattering an α-particle beam from the cyclotron into the magnet system by means of a copper degrader placed at the target position. A portion of the copper degrader was in the form of 45 deg wedges so that the momentum distribution of this degraded beam was flat over a region large compared with the momentum bite of the magnet system. For the first part of the tuning operation, counters T_1 and T_2 were removed and vacuum piping inserted in their place; thus, the entire path through the system was in vacuum except for regions in the vicinity of the degrader and the slits in front of Q_1. The counting rate and beam profiles in the horizontal and vertical planes at the final image position were measured by means of the two 4$\times$4-in. scintillation counters, T_3 and T_4, and a movable 0.5 in.-diam scintillator counter, for various currents in the quadrupoles. The currents were varied in such a way as to

affect the optical properties in only one plane at a time. Optimum transmission was achieved for the calculated current settings in all the quadrupoles. The beam profiles at the final image position were then measured for various collimator configurations in front of Q_1. In each case the measurements agreed very well with the predictions from the ray traces; specifically, the measured and predicted values of the full-width-at-half-maximum of the profiles agreed to within 10%.

Counters T_1 and T_2 were placed into the system in their normal positions (Fig. 3). The currents in M_4 and Q_3 were then adjusted slightly to compensate for the small energy loss of the alphas in these counters and in the windows of the vacuum system in their vicinity. Beam profiles were then measured again. From these profiles, the effect of the multiple scattering in T_1 and T_2 on the transmission of the beam could be determined because the 4×4-in. counters T_3 and T_4, at the final image represent the limiting optical stops for the system beyond the field lens; that is, by the extrapolation of the tails of the profiles to zero, the fraction of the beam scattered out of the system as a result of the presence of T_1 and T_2 is given by the fraction of the total area under the profiles outside the 4×4-in. counters. Because T_1 and T_2 were very thin and were located near optical image points, their presence did not appreciably affect the transmission of particles through the system. Under the operating conditions for data-taking runs (Sec. III), the fraction of the beam that did not traverse the entire counter telescope because of multiple scattering in T_1 and T_2 was determined to be approximately 3% and 10% for magnet-system momenta of 1060 MeV/c and 872 MeV/c, respectively.

E. High-Pressure Gas Target

A schematic diagram of the target is shown in Fig. 11. The target consists of an aluminum cylinder of 0.5 in. -thick walls, 6 in. i. d., and 31.5 in. long, with aluminum domes, 1/32 in. thick and 3 in. in radius, welded to it at either end. The aluminum domes were made as thin as possible (consistent with safety requirements) to minimize the amount of material in the deuteron beam and to minimize the energy loss and multiple scattering of the secondary alpha beam in leaving the target. The gas in the target was cooled to liquid nitrogen temperature, 77°K, by circulating liquid nitrogen through tubing attached to the outside of the cylinder walls. The temperature of the target was measured by means of six thermocouples (copper-constantan) placed about the target. The whole arrangement, target vessel and cooling coils, was enclosed in a vacuum. The pressure of the D_2 and H_2 gas in the target was normally 390 psi (abs), which was the designed pressure limit of the target. The density of the D_2 gas under these conditions was 0.0170 g/cm^3. For the measurement of the γ reaction, (7), at $\Theta_{c.m.} = 135$ deg, the target pressure was reduced to 350 psi (abs) in order to reduce the energy loss of the alphas coming from this reaction, which was considerable because of their lower momentum. The target pressure was measured to within an accuracy of 1.5% by two Bourdon-type gauges connected in the gas entry-and-exit lines. The gas-handling system was designed so that when the target was emptied of deuterium, the gas was recovered and stored in a reservoir for later use. The hydrogen was allowed to escape to the atmosphere.

The geometries of the deuteron and alpha beams at the target are shown in Fig. 4. If we refer to this diagram, it is seen that ray B-1 has a longer path length in deuterium than ray C-5. To correct for this longer path, a wedge of Mylar was placed at the entrance of the first slit. The wedge varied in thickness from 0 g/cm^2 at point I to 0.204 g/cm^2 at point J. With this arrangement, α-particles of the same

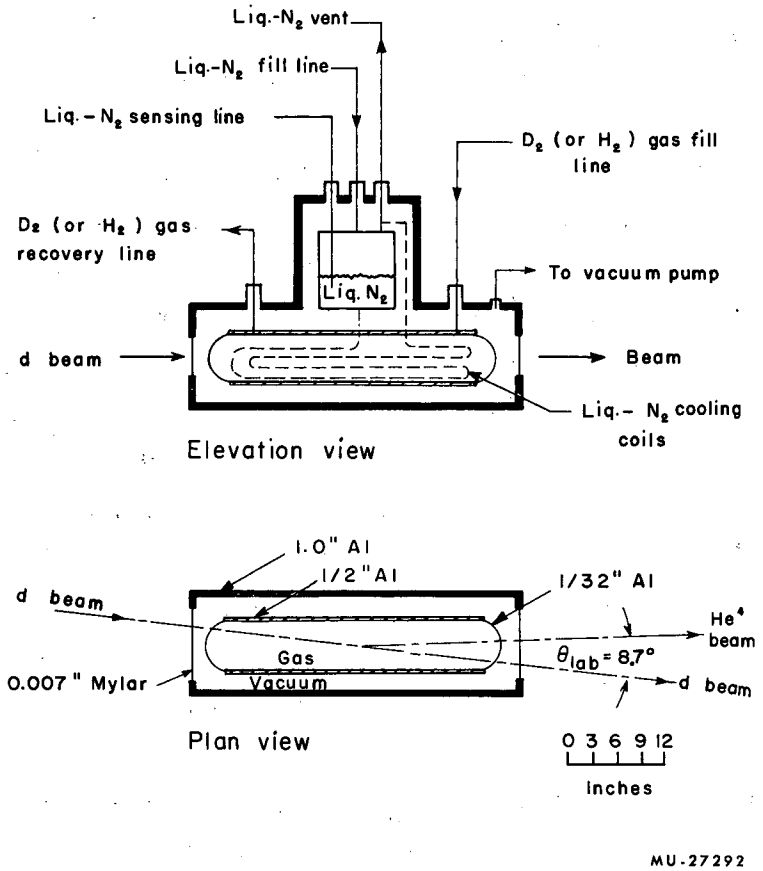

Fig. 11. Schematic diagram of gas target. He^4 beam is at an angle of 2 deg with respect to the target axis in the horizontal plane.

momentum and angle produced at points B, Y, and C will still be equal in momentum at Q_1 because they will have suffered the same energy loss. For the target pressure of 390 psi (abs), the path length in D_2 of the central ray is 0.810 g/cm^2.

F. Counter Telescope

1. Description of the Telescope

The dimensions of the scintillators and their positions relative to the final image position are given in Table I. The counters were made very thin in order to minimize the energy loss and multiple scattering of the α-particles as they passed through. Details of the construction of T_3 and T_4 counters are shown in Fig. 12. Counters T_1, T_2, and A_1 are similar in construction to T_3 and T_4--the only difference being in the size of the scintillator and aluminum foil housing. The R counter was also of the same type as T_3 and T_4 but consisted of two phototubes 180 deg apart. The scintillators were suspended from an Alzac frame by means of fine copper wire and enclosed in a 1.5 mil-thick aluminum foil housing. All the scintillators, except that of the R counter, had one smooth surface and one rough surface. The R counter scintillator had both sides rough. The purpose of the rough surface was to reduce internal reflection of the light in the scintillator by acting as a diffuse surface. The light from the scintillators was reflected onto the photomultipliers by the aluminum foil, as shown in Fig. 12. This method of light collection was considered preferable to the usual method, which uses lucite light pipes, because of the thinness of the scintillators. For such thin scintillators it was felt that (a) more light could be collected, and (b) the light collection would be less position-sensitive, with the former method than with the latter. Each of the counters used was tested for uniformity of response over its entire area by means of a beta source. The variation in pulse height as a function of the beta source position was less than 10%.

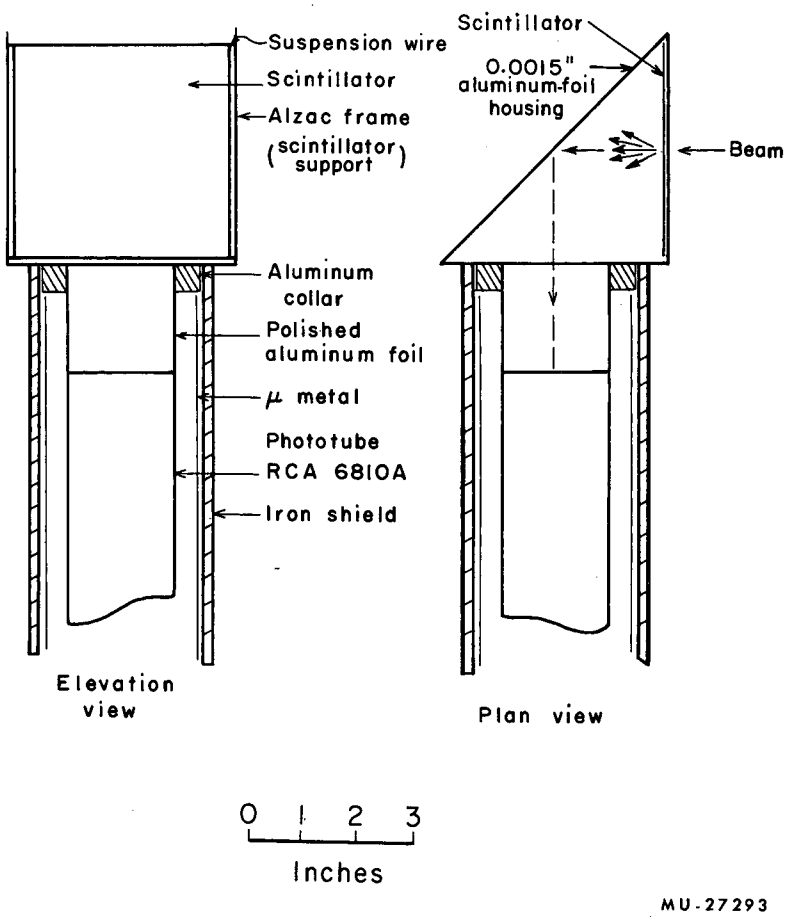

Fig. 12. Schematic diagram of counters T_3 and T_4.

The purpose of the counter telescope was to separate α-particles from other particles with the same P/z selected by the magnet system. Time of flight between T_1, T_2, and T_4 fixed the velocity and therefore the ratio of mass to charge of the particles. Deuterons were then the only contamination remaining. The thickness of the polyethylene absorber (CH_2) between T_4 and A_1 allowed α-particles to be counted in T_4 but not in A_1, whereas deuterons of this P/z had sufficient range to be counted in A_1. Alpha particles were then selected by the coincidence $T_1T_2T_4\overline{A}_1$. Additional identification of alphas was obtained by means of dE/dx. The pulses from T_3 and T_4 were fed into pulse-height discriminators which were set to count pulses above a given pulse-height only. The levels of these discriminators were adjusted to fire on α-particle pulses with ≈ 100% efficiency. The outputs of these discriminators were fed into a coincidence circuit whose output was then placed in slow coincidence with the fast coincidence $T_1T_2T_4\overline{A}_1$. The output of the slow-coincidence circuit was used to trigger a four-gun oscilloscope on which the pulses from each individual counter were displayed. Each time the oscilloscope was triggered, a photograph of the scope display was taken. The information recorded on the film then provided a check of the electronics. Additional dE/dx information was to have been obtained from pulse-height analysis of the R counter; however, during the actual data runs, the singles counting rate (primarily deuterons) in that counter was found to be too high for the pulse-height analyzer and therefore the counter was not used. The telescope had, however, already been calibrated with this counter in place, so it was left in its normal position as part of the absorber arrangement. The counter was removed when the magnet system was set to look for the γ reaction (7), at $\Theta_{c.m.} = 135$ deg because of the small range of the alphas. The dE/dx information obtained from lower-level discrimination of counters T_3 and T_4 was sufficient, since the resolution of these counters was good enough that lower-level discrimination of their pulse heights provided very efficient identification of alphas. (See Sect. II.F.2).

By means of time-of-flight, the contamination in the beam was also measured. Various fast coincidences between T_1, T_2, T_3, and T_4 counted protons, deuterons, and He^3. The numbers of protons and He^3 in the beam were about 5% and 30% that of the deuterons.

A simplified block diagram of the electronics is shown in Fig. 13. Except for the slow-coincidence circuit, all the components are more or less stock items at the Lawrence Radiation Laboratory and are described in the LRL Counting Handbook.[18] The fast coincidence circuits were of the type described by Wenzel.[18,19] Because of the large momentum bite of the α-particles, long clipping lines were used to make the resolving time of these circuits about 18×10^{-9} sec. The slow-coincidence circuit was designed to take output pulses from the 10 Mc pulse discriminators,[18] and provided an output pulse capable of driving a scaler.

2. Calibration of the Counter Telescope

The telescope was calibrated with an α-particle beam from the cyclotron. The beam was scattered into the magnet system by a copper degrader placed at the target position. With the voltage on each counter adjusted to give pulses of about 2 volts into the coincidence circuits, the counters were timed into coincidence. With the counters thus timed, the coincidence rates were measured as a function of the voltages applied to the counters; then, the voltages were set at a value about 100 V greater than the lower edge of the plateau of the resulting curves. The time delays of the counters were adjusted to account for these changes in voltage. Next, the input levels of the 10 Mc discriminators that take the output of the fast coincidence circuits were adjusted by measuring the coincidence output rates as a function of discriminator level; the input levels were set at a value safely on the plateau of the curve. The input levels of the 10 Mc lower-level discriminators on counters T_3 and T_4 were determined by measuring the α-beam singles counting rate in T_3 and T_4 as a function of the respective discriminator level, and setting the level on the plateau of the curve. Finally, the amount

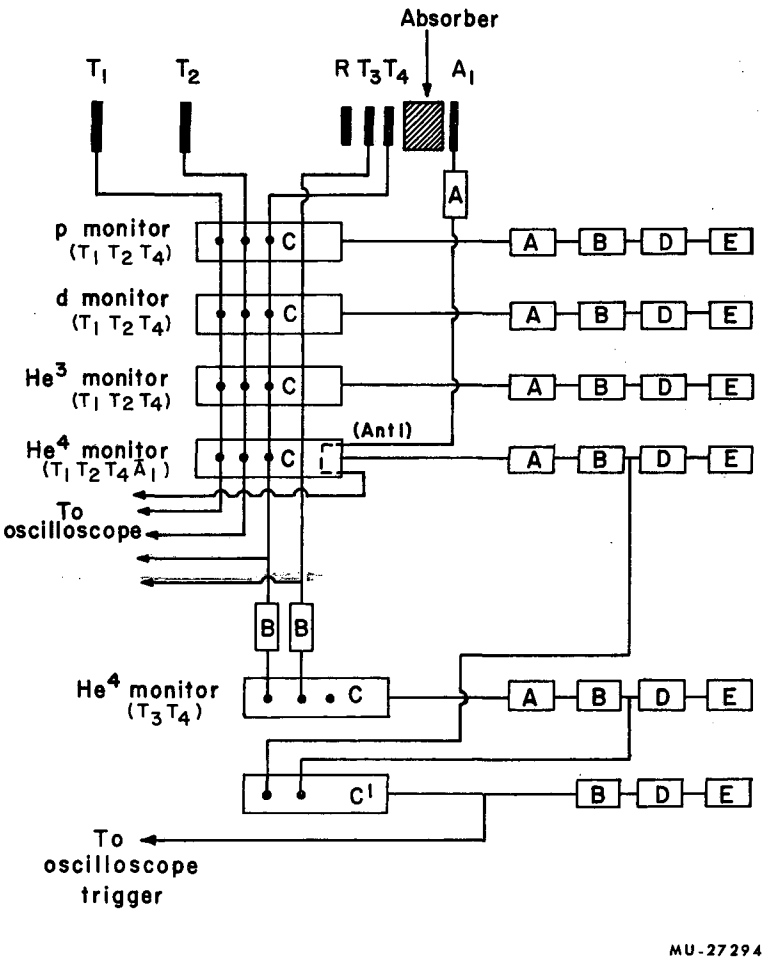

Fig. 13. Block diagram of electronics. A. Wide-band amplifier. B. Discriminator. C. Fast coincidence circuit. C^1. Slow coincidence circuit. D. Fast pre-scalar. E. Decade scalar.

of CH_2 absorber was determined by measuring the coincidence rate $T_1T_2T_4\bar{A}_1$ as a function of absorber thickness. The absorber curves obtained with the magnet system set for α-particle momenta of 1060 MeV/c and 872 MeV/c are shown in Fig. 14. The absorber thicknesses used in the data-taking runs are shown there. These curves are consistent with the calculated momentum spectrum transmitted by the magnet system (Fig. 10).

A measure of the telescope efficiency was obtained from a comparison of the telescope counting rate with the α-particle singles counting rate in T_3 and T_4. With a low-intensity α-beam from the cyclotron (about 0.2% of maximum) the singles counting rate in T_3 and T_4 was measured with their lower-level discriminators set at a low firing level. Their counting rates were the same within statistics. The counting rate of the α-particle telescope was then measured with all its components set at their plateaued values. The ratio of the latter to the former counting rates was $96 \pm 5\%$. The error on this number is a measure of the counting rate statistics and the uncertainty in the absolute efficiencies of the T_3 and T_4 counters. This number is a lower limit on the telescope efficiency because any background in the blockhouse surrounding T_3 and T_4 would have made the singles counting rate in these counters higher than the true α-beam counting rate.

With the use of a deuteron beam from the cyclotron, the various counters were also timed into fast coincidence circuits to measure protons, deuterons, and He^3 by time of flight.

During the experiment, the cross section for deuterons on carbon,

$$d^2\sigma/\, d\Omega dp(d + C^{12} \rightarrow He^4 + \text{residue}),$$

was also measured by using the CH_2-H_2 subtraction technique. The result is 0.38×10^{-30} cm^2/sr-MeV/c for α-particles of 1060 MeV/c lab momentum and lab angle of 8.7 deg. Using the CH_2 target, we

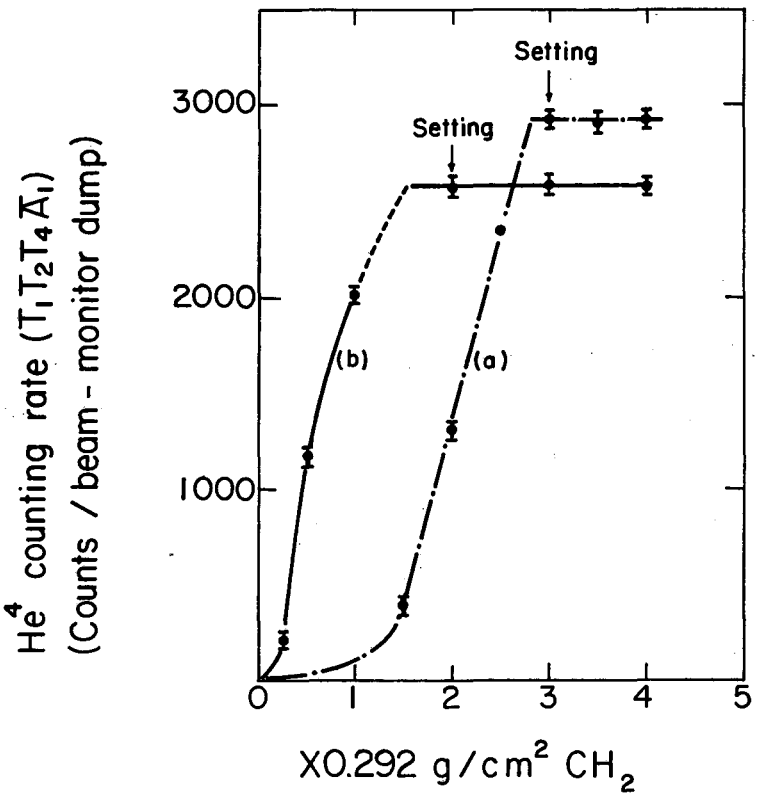

Fig. 14. Absorber curves. (a) Magnet-system momentum $P(He^4)$ = 1060 MeV/c. (b) Magnet-system momentum $P(He^4)$ = 872 MeV/c. Dashed portion obtained by extrapolating solid lines.

could show that the electronics did not saturate even though the production cross section for α-particles and the background of deuterons were larger than with the deuterium target in place. The counting rate was measured as a function of beam intensity; a least-squares fit of data showed that the electronics was linear to within ± 5%. The efficiency of the telescope for the data-run conditions was taken to be equal to the product of the efficiency measured at low alpha-beam intensity and the linearity factor determined with the CH_2 target. The result is

$$\text{efficiency} = (96 \pm 7.2)\% .$$

During the data runs, consistency checks of the α-counter telescope system were made periodically with an α-particle beam from the cyclotron degraded at the gas target.

III. COLLECTION OF DATA

We looked for the π^0 reaction (5) by taking a series of data runs; the target gas was cycled between deuterium and hydrogen at a pressure of 390 psi(abs) and the magnet system was set at the corresponding α-particle momentum of 1060 MeV/c. Alphas having this momentum at the magnet system had a momentum of 1275 MeV/c at the target center. The range of these alphas in D_2 at the target center was 2.31 g/cm^2. For this momentum setting, the α-particle-selecting magnet system was sensitive to the production of a neutral particle with a mass of 120 to 155 MeV.

To investigate the γ reaction, (7), at $\Theta_{c.m.} = 65$ deg for the same target pressure (390 psia), the magnet system would have to be set for an α-momentum of 1274 MeV/c. Alphas having this momentum at the magnet system had a momentum of 1427 MeV/c at the target center. The range of these alphas in D_2 at the target center was 3.43 g/cm^2. However, because of magnet power-supply limitations at the 184-inch cyclotron, the maximum α-momentum the system could accept was 1150 MeV/c. Therefore, to look for the γ reaction with this experimental setup, it was necessary to degrade the alphas to a momentum $\leq$ 1150 MeV/c. Thus, 1.03 g/cm^2 of CH_2 was placed in the beam at the entrance of the collimator to degrade the alphas to a momentum of 1060 MeV/c. With this magnet momentum and the same target pressure setting as above, a series of data runs was taken with the target gas cycled between deuterium and hydrogen. For this setup, the system was sensitive to the production of a neutral particle of mass 0 to 110 MeV.

Additional information about the γ reaction and about background was obtained by setting the system to look for the latter reaction at $\Theta_{c.m.} = 135$ deg. With the degrader removed, the target pressure reduced to 350 psi (abs), and the magnet system set correspondingly at 872-MeV/c alpha momentum, data runs were taken with deuterium and then hydrogen in the target. The reason for the reduced target pressure

was to reduce the energy loss of the alphas since the range of these alphas at the target center is only 1.55 g/cm^2 in D_2. For purposes of normalization at this magnet momentum, the measurements for the π^0 reaction described above were repeated with 0.525 g/cm^2 CH_2 added at the entrance of the magnet-system collimator to degrade the alphas to 872 MeV/c. For these measurements and for those of the γ reaction at $\Theta_{c.m.} = 135$ deg, the R counter was removed from the system because of the small range of the alphas.

To investigate the effect of possible α-particle contamination of the incident deuteron beam, we scattered an α-beam (from the cyclotron) off the target, and measured the α-particle counting rate in our system under the same conditions in which the π^0 reaction and the γ reaction at $\Theta_{c.m.} = 65$ deg were measured. In both cases, the α-d inelastic scattering yielded 1.48$\pm$0.03 times as many α-particle counts as did α-p scattering. Thus, alpha contamination of the deuteron beam from the cyclotron or from deuteron interactions upstream from the target would provide a net positive difference in α-particle yield between the deuterium and hydrogen targets.

Possible alpha background produced from deuteron interactions in the target window was investigated by placing 0.090-in. Al at the target entrance and taking a short data run with D_2 gas in the target and with the system set for the π^0 reaction. The α-particle counting rate showed an increase of about 10% over the rate with the additional Al foil removed; however, the errors are large.

IV. DATA ANALYSIS AND RESULTS

A. Electronics Data and Oscilloscope Film Analysis

The electronics data are presented in Table II. The indicated errors are statistical.

As a check of these data, the photographs of the oscilloscope display were analyzed. From these pictures the pulse-height distribution of each counter output and the timing between the counters could be measured. To calibrate the scope display, an alpha beam from the cyclotron was scattered into the magnet system and scope pictures were taken with the scope triggered by the alpha-telescope electronics (Fig. 13). Then, with a deuteron beam, calibration pictures of deuteron, He^3, and proton events were taken by triggering the scope with the output of the time-of-flight coincidence circuits for d, He^3 and p, respectively. The timing between pulses from the T_1 and T_3 counters is proportional to the horizontal distance between them. Histograms of the timing between these counters for the various calibration runs are shown in Fig. 15; from this it is seen that the scope display provides very good timing separation between He^4, He^3 and p. A scan of the pictures of the actual data, for the magnet system set at 1060 MeV/c alpha momentum, shows that all the events have a timing that corresponds to that of alphas or deuterons (these particles have the same velocity for a given magnetic rigidity); moreover, no pulses from the anticounter, A_1, are seen. Thus, all the events have the timing and range of alphas.

However, an analysis of the pulse heights of the counters shows that only a small fraction of these events are, in fact, α-particles. The pulse-height distribution of each counter, obtained from the oscilloscope pictures, is shown in Fig. 16(a). The distributions obtained with the system set to look at the π^0 or γ reactions and using the D_2 or H_2 target are very nearly the same; as a result the data of all the

Table II. Electronics data. Counts per 10^{13} deuterons incident on target.

Case	Magnet momentum, $P(He^4)$ (MeV/c)	$P(He^4)$ at target center (MeV/c)	Alpha counts from target			Deuteron counts from target[a]	
			D_2	H_2	Empty	D_2	H_2
$d + d \rightarrow He^4 + \pi^0$	1060	1275	62.2±1.69	45.0±1.41		63×10^3	44×10^3
$d + d \rightarrow He^4 + \gamma$	1060	1427	67.2±2.11	47.8±1.82		62×10^3	44×10^3
Target empty background	1060	1140			32.7±2.14		
$d + d \rightarrow He^4 + \pi^0$	872	1275	21.6±1.75	12.3±1.13			
$d + d \rightarrow He^4 + \gamma$	872	1150	25.2±1.41[b]	14.5±0.85[b]			

[a] Counter telescope was not plateaued for counting deuterons; therefore numbers should be considered only as indicative.

[b] Counting rate corrected for reduced target pressures; that is, counting rate normalized to target pressure of 390 psi (abs).

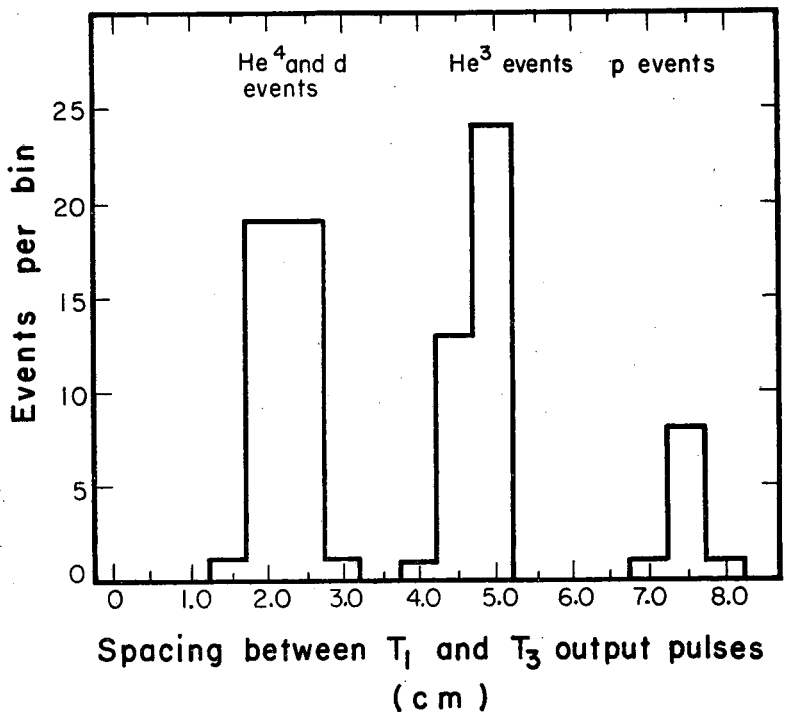

Fig. 15. Calibration timing distribution from oscilloscope film traces. The horizontal scale is arbitrary. The significant information is the separation between the histograms since this quantity is proportional to the difference in transit time between T_1 and T_3 for the respective particles. Magnet system momentum set at $P(He^4) = 1060$ MeV/c.

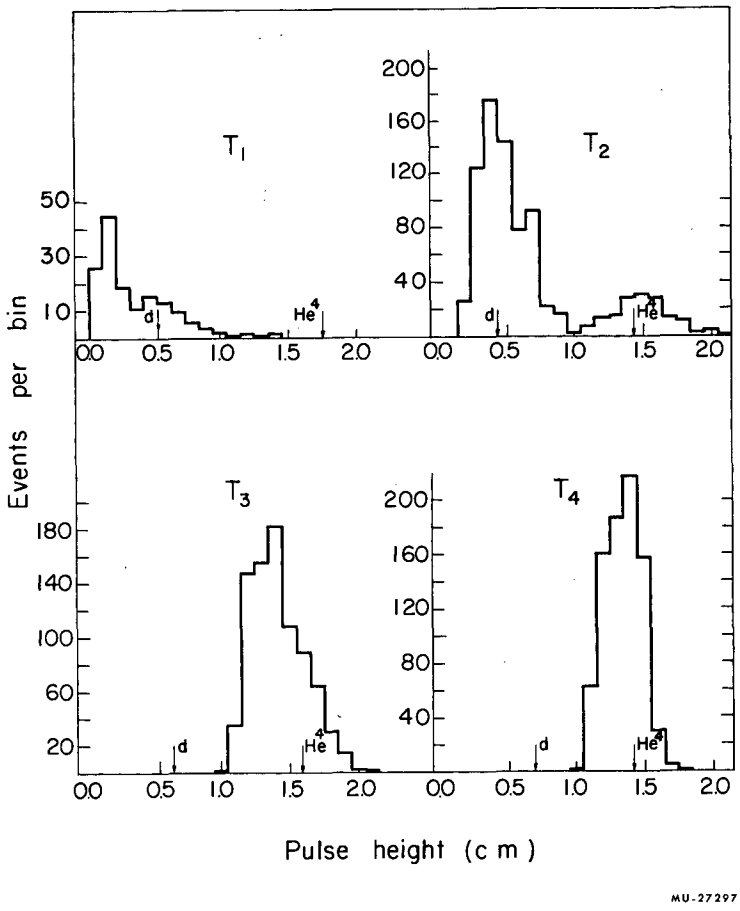

Fig. 16(a). Pulse height spectra determined from oscilloscope film for magnet-system momentum P(He^4) = 1060 MeV/c. Spectrum of T_1 counter output is based on a scan of only a few events (160): spectra of the other counter outputs are based on a scan of approximately one-third of all the data. Arrows indicate medians of the calibration pulse height spectra for d's and He^4's obtained with d and He^4 beams, respectively, from the cyclotron.

settings have been combined. Except for the T_1 counter, the pulse-height data are based on a scan of approximately one-third of all the events. The pulse-height spectrum for counter T_1 shows that it was "sagging" badly; this was because it was located in a region of high background. For purposes of time-of-flight coincidences, however, T_1 was shown to be counting alphas efficiently. The distributions for T_3 and T_4 each show a single broad peak, the center of which is at a slightly lower pulse height than that of the calibrated alpha distribution. The low pulse-height edges of the distributions for these two counters correspond to the lower-level discriminator cutoff. The T_2 counter pulse-height spectrum has two well separated peaks; the higher pulse-height peak position coincides with that of the alpha calibration peak, and the lower peak with the calibrated deuteron spectrum. In Fig. 16(b), pulse-height spectra of T_1, T_3, and T_4 counters are plotted for the events in which the T_2 pulse height occurs in the higher peak and lower peak, respectively. From these graphs, it is seen that the pulse-height spectra in the counters are correlated. For the events in which the T_2 pulse height corresponds to that of alphas, the output of counters T_3 and T_4 also corresponds to that for alphas; however, for those events which have a deuteron pulse height in T_2, the pulse-height distributions for T_3 and T_4 are peaked about a pulse height lower than for alphas. This information, together with the fact that the timing for all the events is the same (within the resolution of the coincidence circuits), indicates that most of the events which the electronics recorded as alphas were really deuterons; these deuterons had somehow been converted near the final counters to particles which produced a large pulse height in T_3 and T_4 and which had sufficiently low range to be absorbed before reaching the anti counter A_1. The only material in the beam upstream from and near the final counters was the R counter and the 0.010-in.-thick Mylar window of the vacuum system.

From the calibration pulse height data and from the formula of Gooding and Pugh,[20] we calculated the pulse height as a function of energy loss in the counters. With this information, the kinetic energy required of various particles to give the pulse height of the lower peak in T_3 was calculated; the results are listed in Table III.

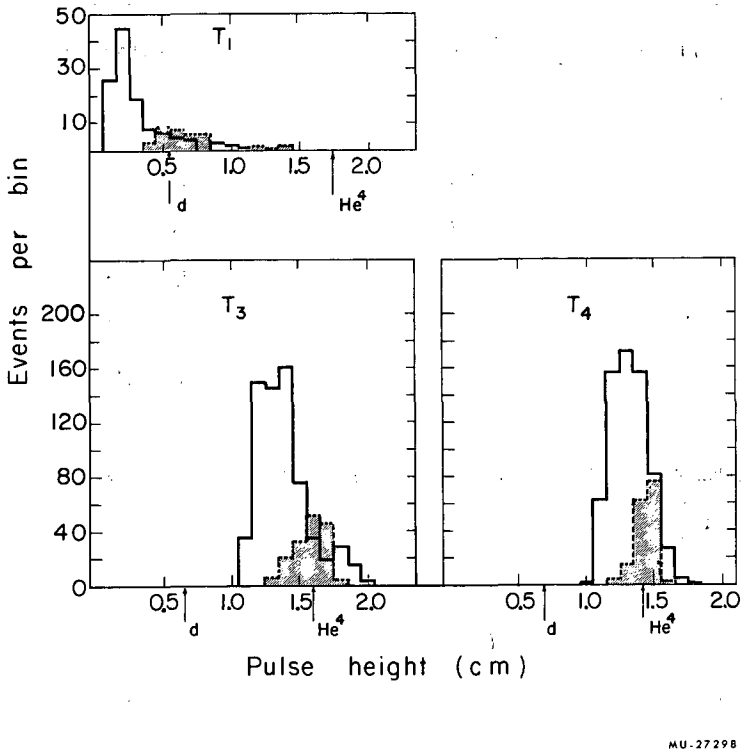

Fig. 16(b). Correlated pulse height spectra of data in Fig. 16(a). Cross hatched histogram is the spectrum for events in which the T_2 pulse height occurs in higher peak (i.e., T_2 p.h. $\geq$ 1.0 cm., cf. Fig. 16(a)). Clear histogram is the spectrum for events in which the T_2 pulse height occurs in the lower peak (i.e., T_2 p.h. $\leq$ 0.9 c.m., cf. Fig. 16(a)). Arrows indicate medians of the calibration pulse height spectra for d's and He^4's.

Table III. Calculated kinetic energies for various particles corresponding to pulse heights from counter T_3.

Particle	Kinetic energy (MeV)	Velocity ($\beta = v/c$)	Range in CH_2 (g/cm^2)
(a) Kinetic energies corresponding to median pulse height of lower peak.			
He^4	240	0.34	2.83
He^3	177	0.34	2.05
H^3	33	0.159	0.39
d	24	0.159	0.30
p	11.5	0.159	0.14
(b) Maximum kinetic energies accepted by lower-level discriminator on T_3.			
H^3	45	0.177	0.68
d	30	0.177	0.45
p	15	0.177	0.23

Remarks: Incoming deuteron beam has kinetic energy of 72 MeV ($\beta = 0.27$) at R counter. Thickness of CH_2 absorber in front of counter $A_1 = 0.876$ g/cm^2.

From the numbers in Table III, it is seen that, on the basis of energy conservation and range, the lower pulse height peak in T_3 and T_4 cannot be caused by He^4 or He^3 particles coming from a deuteron-carbon reaction in the R counter and Mylar vacuum window; the effect may be due, however, to H^3, inelastic deuterons, or protons produced in the deuteron-carbon reaction. The experiments of Schechter et al,[21] and Milburn et al.[22] on d-C^{12} scattering at 190 MeV and 160 MeV, respectively, indicate that protons produced from deuteron stripping would be the dominant contribution. From the data in Table II and the oscilloscope film results, the cross section of a d-C^{12} reaction (in the R counter and Mylar vacuum window) to produce these singly charged particles of $\beta \leq 0.177$ in the solid angle subtended by T_3 and T_4 counters, was calculated and the result is $\frac{d^2\sigma}{dPd\Omega}\ \Delta P \Delta\Omega \approx 90$ mb; that is, a cross section of this magnitude would account for all the counts in the lower pulse-height peak in T_3 and T_4. This cross section is consistent with the results of Schechter et al.,[21] extrapolated to a deuteron kinetic energy of 72 MeV.

From an analysis of the kinematics of d-p elastic scattering, it can be concluded that protons or deuterons from the elastic scattering of deuterons with the hydrogen in the R counter scintillator and the Mylar window cannot contribute to the above effect; that is, in the lab angle interval subtended by the T_3 and T_4 counters, the elastically scattered protons or deuterons do not have the kinetic energies required to give the observed pulse-height spectra in T_3 and T_4.

To determine the number of true alpha counts for the data runs with the magnet system set for 1060-MeV/c alphas, we scanned every event on the oscilloscope film and recorded the number of events for which the T_2 counter pulse height corresponded to that of alphas. The results are shown in Table IV.

Table IV. Oscilloscope film data. True alpha counts per 10^{13} deuterons incident on target.

Case	Magnet momentum $P(He^4)$ (MeV/c)	$P(He^4)$ at target center (MeV/c)	Alpha counts from target[a]		
			D_2	H_2	Empty
$d+d \rightarrow He^4 + \pi^0$	1060	1275	12.7±0.77	9.1±0.65	
$d+d \rightarrow He^4 + \gamma$	1060	1427	15.5±1.10	10.5±0.82	
Target empty background	1060	1140			9.6±1.16
$d+d \rightarrow He^4 + \pi^0$	872	1275	8.1±1.07	4.4±0.59	
$d+d \rightarrow He^4 + \gamma$	872	1150	9.3±0.82[b]	5.3±0.53[b]	

[a] Errors are statistical.

[b] Counting rate corrected for reduced target pressure.

The pulse-height spectra from T_2, T_3, and T_4 with the magnet system set for 872-MeV/c alphas are shown in Fig. 17. As in the 1060 MeV/c cases, the spectra show that most of the events recorded as alphas by the electronics are really products from deuteron-carbon reactions. In this case, however, the reaction occurred only in the Mylar vacuum window, since the R counter had been removed for the data runs at this magnet momentum setting. The numbers of true alpha counts, as determined from the film scan, are included in Table IV.

B. Acceptance of the Magnet System

To calculate the cross sections for the π^0 and γ reactions the acceptance of the system must first be determined. In this context, the acceptance is defined as follows:

$$\text{Acceptance} = (\Delta\Omega_{\text{c.m.}}^{\text{eff}})\,(t^{\text{eff}})\,(M), \tag{8}$$

where $\Delta\Omega_{\text{c.m.}}^{\text{eff}}$ = effective solid angle in the center-of-mass system subtended by the collimator and magnet system (this quantity is a function of the configuration of the magnet-system collimator, the momentum bite of the magnet system, and the kinematics of a particular reaction),

t^{eff} = effective thickness of the target seen by the magnet-system collimator, in cm,

M = probability of the α-particle being accepted by the magnet-system collimator as a result of multiple scattering in the target.

The acceptance is evaluated by means of a numerical integration, which is described in detail in Appendix B. The results are shown in Table V.

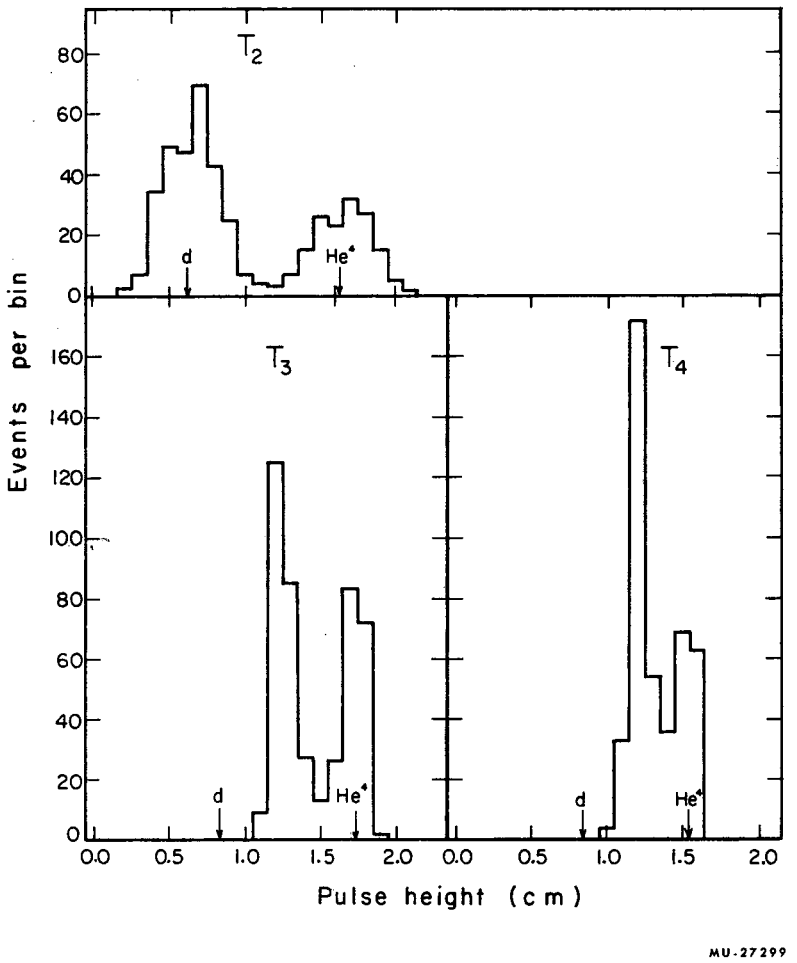

Fig. 17. Pulse height spectra determined from oscilloscope film for magnet-system momentum P(He^4) = 872 MeV/c. Spectra include approximately one-half of all the data. The pulse heights of the various counters are correlated. Arrows indicate medians of the calibration pulse height for d's and He^4's.

Table V. Acceptance of the magnet system.

Reaction	Magnet momentum, $P(He^4)$	
	1060 MeV/c	872 MeV/c
$d + d \rightarrow He^4 + \pi^0$ (about $\Theta_{c.m.} = 90$ deg)	0.790 sr-cm	0.280 sr-cm
$d + d \rightarrow He^4 + \gamma$ (about $\Theta_{c.m.} = 65$ deg)	0.468 sr-cm	
$d + d \rightarrow He^4 + \gamma$ (about $\Theta_{c.m.} = 135$ deg)		0.293 sr-cm

C. Calculation of the Cross Sections and Results

Because the conservation of baryon number forbids the production of α-particles from d-p collisions, the hydrogen data are treated as background and subtracted from the deuterium data to yield the net He^4 signal from d-d collisions. However, this signal is to be considered as an upper limit for the following reasons.

1. Any α-particle contamination of the deuteron beam from the cyclotron or from deuteron interactions upstream from the target would provide a net positive yield. As mentioned in Sec. III, this possibility was investigated by measuring the α-particle yield into the counter telescope for the case of an α-beam from the cyclotron incident on the deuterium and hydrogen targets. The α-d inelastic scattering yielded 1.48±0.03 times as many alpha counts as did α-p scattering.

2. From the data in Table II, it is seen that more inelastic deuterons scatter into the system from the deuterium target than from the hydrogen target. Thus, it is conceivable that if some of the deuterons interacted at the target walls to produce alphas, a net positive yield of alphas would result from a D_2-H_2 substraction of the data.

3. The increase in alpha counting rate obtained when 0.090-in. Al was placed in the beam at the target entrance--although not conclusive because of the large errors--is consistent with the alpha counting rate obtained from the D_2-H_2 subtraction of the data for the π^0 and γ reactions. This would indicate that the production of alphas from d-Al interactions at the target window and their subsequent scattering in the target gas (reason 1), may account for the net positive yield of alphas obtained from a D_2-H_2 subtraction of the data. Further background analysis is discussed in the following paragraphs.

To get a firm upper limit for the π^0 reaction, we consider only the data obtained with magnet momentum set at $P(He^4)$ = 1060 MeV/c and assume that the alpha counts in Table IV for the D_2 target minus those from the H_2 target were caused entirely by the π^0 reaction. The cross section is then calculated from the formula

$$N = N_i \cdot \rho_t \left[(\Delta\Omega_{c.m.}^{eff})(t^{eff})(M) \right] E \cdot (1-X) \cdot \frac{d\sigma_{cm}}{d\Omega}, \qquad (9)$$

where N = number of net alpha counts per 10^{13} incident deuterons,

$N_i = 10^{13}$ deuterons,

ρ_t = density of target in atoms/cm^3 = 5.06×10^{21} atoms/cm^3,

$\left[\Delta\Omega_{c.m.}^{eff} (t^{eff})(M) \right]$ = acceptance by system, in sr-cm,

E = efficiency of counter telescope = (96±7.2)%,

and

X = fraction of the alpha signal that did not pass through the entire telescope because of multiple scattering in T_1 and T_2 counters = 0.03 for magnet system momentum of $P(He^4)$ = 1060 MeV/c.

From the foregoing we obtain, for the reaction $d+d \rightarrow He^4+\pi^0$ at about 90 deg (c.m.),

$$\left(\frac{d\sigma}{d\Omega}\right)_{c.m.} = (0.97 \pm 0.27) \times 10^{-34} \text{ cm}^2/\text{sr}. \qquad (10)$$

Because this is to be considered as an upper limit, we increase the value by two standard deviations and quote the limit as

$$\left(\frac{d\sigma}{d\Omega}\right)_{c.m.} < 1.5 \times 10^{-34} \text{ cm}^2/\text{sr}. \qquad (11)$$

To get an upper limit on the degree of nonconservation of isotopic spin in strong interactions, this value is compared with the theoretical prediction for the cross section[3] which was computed with the assumption that isotopic spin need not be conserved. The theoretical value is

$$\left(\frac{d\sigma}{d\Omega}\right)_{c.m.}^{theoret} = (380 \pm 50) \times 10^{-34} \text{ cm}^2/\text{sr}. \qquad (12)$$

The ratio of Eq. (10) to Eq. (12), increased by two standard deviations, equals 0.004; that is,

$$\text{probability of nonconservation of isotopic spin} < 0.4\%, \qquad (13)$$

or, alternatively, isotopic spin in strong interactions is at least 99.6% conserved.

With the same procedure outlined above, the upper limit for the c.m. differential cross section for the reaction $d+d \rightarrow He^4+\gamma$ at $\Theta_{c.m.} = 65$ deg was calculated; the value is

$$\left(\frac{d\sigma}{d\Omega}\right)_{c.m.} (65 \text{ deg}) < 3.5\times 10^{-34} \text{ cm}^2/\text{sr}. \qquad (14)$$

This value is a two-standard-deviation limit, the standard deviation being 0.61×10^{-34} cm^2/sr. From this, one can get an upper limit for the total cross section for the γ reaction. For this reaction, the electric dipole transition is forbidden and the most probable transition is the electric quadrupole transition, $^1D \rightarrow {}^1S$,[5,23] which would make the angular distribution of the form $\sin^2\Theta_{c.m.} \cos^2\Theta_{c.m.}$.[5] For this angular distribution, the upper limit for the total cross section is

$$\sigma_t(d + d \rightarrow He^4 + \gamma) < 4.0\times10^{-33} \text{ cm}^2. \qquad (15)$$

To determine whether or not the cross sections for these reactions are nonzero, a D_2-H_2 subtraction of the data at one momentum for either reaction is not sufficient (for reasons mentioned above). From the data obtained at magnet-system momentum of $P(He^4) = 872$ MeV/c, together with the 1060-MeV/c data, the effect of the possible sources of background can be determined and the true cross sections calculated. This background analysis is described in Appendix C.

The set of equations described there includes the possible background terms which do not cancel out in a D_2-H_2 subtraction of the data. From these equations the true α-particle signals for the π^0 and γ reactions were derived; the results are

(a) For $d+d \rightarrow He^4+\pi^0$ (about $\Theta_{c.m.} = 90$ deg),

$$\left(\frac{d\sigma}{d\Omega}\right)_{c.m.} = (-3.4\pm3.1)\times10^{-34}\ cm^2/sr; \qquad (16)$$

and

(b) For $d+d \rightarrow He^4+\gamma$ ($\Theta_{c.m.} = 65$ deg),

$$\left(\frac{d\sigma}{d\Omega}\right)_{c.m.} = (1.4\pm1.3)\times10^{-34}\ cm^2/sr. \qquad (17)$$

The results are consistent with zero cross sections for both reactions. We find, therefore, no evidence of the nonconservation of isotopic spin.

To determine more accurately whether or not the cross sections for these reactions are really nonzero, one needs more accurate information about the background than could be obtained with the setup used in this experiment. Ideally, the most direct and accurate way to investigate the background would have been to measure the α-particle counting rate in the counter telescope as a function of the magnet-system momentum as it was varied in a region from just below to just above that momentum corresponding to the reaction being investigated; this should be done with both the deuterium and hydrogen targets. Such a procedure could not be followed here because the large momentum bite of the magnet system was comparable to the separation in momentum between alphas from the π^0 and γ reactions in this lab angle interval (Fig. 2); that is, if the magnet-system momentum had been set at a value just below or above that for the π^0 reaction (5), the magnet system could have accepted alphas from the γ reaction (7), and vice versa. Additionally, for Reaction (7), at magnet momenta lower than that for Reaction (7)

at $\Theta_{c.m.}$ = 135 deg, multiple scattering and absorption effect became severe because of the low energy of the alphas; thus the background in this region could not be measured effectively. Also, for the region of momenta above that corresponding to $\Theta_{c.m.}$ = 65 deg, the background could not be studied because the magnet currents required were unattainable because of power-supply limitations. Under the circumstances, then, information about background could be derived only by the more indirect method described in Appendix C.

V. CONCLUSIONS

From the results of the experiment we draw the following conclusions:

1. Isotopic spin is at least 99.6% conserved in strong interactions.

2. We find no evidence of nonconservation of isotopic spin in strong interactions. This also means that no evidence was found for the existence of the reaction $d + d \rightarrow He^4 + \pi_0{}^0$, where the $\pi_0{}^0$ is a neutral meson[24] of zero isotopic spin with a rest mass in the interval 120 to 155 MeV. If the $\pi_0{}^0$ exists, then this reaction, which is a strong interaction, would not be forbidden by isotopic spin conservation and therefore should have been detected. For a $\pi_0{}^0$ of the same mass as that of the ordinary π^0, we find $d\sigma^{cm}/d\Omega\,(d + d \rightarrow He^4 + \pi_0{}^0) < 1.5 \times 10^{-34}$ cm^2/sr at $\Theta_{c.m.} \approx 90$ deg.

3. The upper limit of the cross section for the reaction $d + d \rightarrow He^4 + \gamma$ is of the same order of magnitude as that for the reaction $d + d \rightarrow He^4 + \pi^0$.

ACKNOWLEDGMENTS

This experiment was performed with the help of many men and to them I offer my heartfelt thanks for their magnificent effort. In particular, I should like to thank Dr. John A. Poirier for suggesting the problem and for his aid and encouragement in all phases of the experiment; in addition, I am grateful to my colleagues, Mr. William C. Bowman and Mr. Jim B. Carroll, for their significant assistance before and during the experiment and to Messrs. Dale Dickinson, Don Hagge, Richard Eandi, and Alex Maksymowicz for their substantial efforts while the experiment was in progress.

Mr. James Vale and the cyclotron crew are to be commended for their efficient operation of the 184-inch cyclotron. I should also like to pay tribute to the ingenuity and competence of Mr. Lou Sylvia and Mr. Bob Walton and their crew of accelerator technicians in designing and building some of the experimental apparatus.

The efforts of Miss Miriam Machlis in typing the preliminary manuscript are greatly appreciated.

Finally, I should like to thank Professor Burton J. Moyer for his guidance and kindly encouragement during my years as a graduate student. I consider it a singular privilege to have been a student in his group.

This work was done under the auspices of the U. S. Atomic Energy Commission.

APPENDICES

A. SEM Calibration Calculation

The multiplication factor of the ion chamber (I. C.) for a deuteron beam is calculated from the expression[25]

$$M_{I.C.} = \frac{t}{w}(-dE/dx), \tag{A-1}$$

where

$M_{I.C.}$ = ion chamber multiplication factor = number of ion pairs created per incident deuteron particle,

t = amount of argon gas (g/cm^2),

w = specific ionization of argon = 25.5 eV/ion pair,

and

$-dE/dx$ = energy loss of deuterons in argon ($eV/g/cm^2$).

For our case,[26] $t = (9.71 \pm 0.08) \times 10^{-3}$ g/cm^2, and $(-dE/dx) = 2.94 \times 10^6$ $eV/g/cm^2$.

Substituting these values into (A-1), we get

$$M_{I.C.} = (1.120 \pm 0.009) \times 10^3 \text{ ion pairs per incident deuteron.} \tag{A-2}$$

Then, the number of incident deuterons per μC of ion-chamber integrated current, N_d, is given by

$$N_d = \frac{10^{-6}}{e} \times \frac{1}{M_{I.C.}}, \tag{A-3}$$

where e = electron charge in Coulombs.

Therefore,

$$N_d = (0.557 \pm 0.004) \times 10^{10}. \tag{A-4}$$

From the beam intensity measurements in the region where the ion chamber response is linear with intensity, we obtain

$$\frac{\text{SEM current}}{\text{I. C. current}} = (8.86 \pm 0.16) \times 10^{-4} \qquad \text{(A-5)}$$

The multiplication factor for the SEM, M_{SEM}, is defined as the number of secondaries created in the SEM per incident deuteron, and is determined from (A-4) and (A-5):

$$M_{SEM} = (\text{integrated SEM current}/\mu\text{C of I. C. current}) \times \frac{1}{e} \times \frac{1}{N_d}$$
$$= 0.990 \pm 0.015 \text{ secondaries per primary deuteron.} \qquad \text{(A-6)}$$

Therefore,

$$\text{Number of deuterons/sec per } \mu\text{A SEM current} = \frac{1}{M_{SEM}} \times \frac{10^{-6}}{e}, \qquad \text{(A-7)}$$

and the beam intensity at the target is equal to this number increased by 6% to correct for beam loss between the target and the SEM; that is,

$$\text{beam intensity at target per } \mu\text{A SEM current}$$
$$= \frac{1}{M} \times \frac{10^{-6}}{e} \times 1.06$$
$$= (0.67 \pm 0.01) \times 10^{13} \text{ deuterons/sec.} \qquad \text{(A-8)}$$

B. Calculation of the Magnet-System Acceptance

Because the magnet system collimator views an extended target and not a point source, the acceptance by the system, as defined in Sec. IV.B., was evaluated by means of a numerical integration of the following expression,

$$\text{Acceptance} = \iiint M(\Theta_{c.m.}, \phi_{c.m.}, x)\, T(\Theta_{c.m.}) \sin\Theta_{c.m.}\, d\Theta_{c.m.}\, d\phi_{c.m.}\, dx, \tag{B-1}$$

where $\Theta_{c.m.}$ = polar scattering angle in the c.m. system (the polar angle here is measured in the horizontal plane);

$\phi_{c.m.}$ = azimuthal angle in the c.m. system;

x = position coordinate along the incident deuteron beam center line in the target;

$M(\Theta_{c.m.}, \phi_{c.m.}, x)$ = probability that an α-particle, produced at x with angles $\Theta_{c.m.}$ and $\phi_{c.m.}$, is accepted by the magnet system collimator after multiple scattering in the target; and

T = transmission of the magnet system (Sec. II. D.4) and is a function of the momentum of the α-particles; however, since the $\Theta_{c.m.}$ of an α-particle produced in the d-d reaction is uniquely related to the particle's momentum by the kinematics of the reaction, the transmission can be expressed as a function of $\Theta_{c.m.}$.

The term $M(\Theta_{c.m.}, \phi_{c.m.}, x)$ was determined in the following way: Because the path length of the α-particles in the D_2 gas is large, the effect of multiple scattering in the gas could change the spatial distribution of the α-particles as well as their angular distribution. The lateral displacement of the α-particles in the gas as a result of multiple scattering, was calculated by the formula of Rossi [27] and found to be

negligible compared with the beam and collimator dimensions. The mean-square multiple-scattering angles in the D_2 gas, the Al exit window of the target, and the degrader material (if any) at the target exit were calculated by the formula of Bethe and Ashkin,[28] with the total mean-square angle being the sum of these. (For the π^0 reaction the mean square multiple scattering angle for the central ray was 144×10^{-6} rad^2). With the mean-square angle obtained, the probability that α-particle that orginated from $(x, \Theta_{c.m.}, \phi_{c.m.})$ would be multiple-scattered at the target exit into the collimator can then be calculated.[28] Because the r.m.s. multiple-scattering angle was much smaller than the angle subtended by the aperture of Q_1 at the target exit in the azimuthal plane, the effect of multiple scattering in this plane was negligible and only the effect in the horizontal plane was considered.

The acceptance of the system was then calculated in the following way for a particular reaction. From a point x, along the deuteron beam center line in the target, a number of rays were drawn toward the target exit at lab angles corresponding approximately to every 3 deg in the c.m. system about the central $\Theta_{c.m.}$ of the reaction seen by the magnet system. The probability, $M(\Theta_{c.m.}, x)$ of each ray's multiple scattering at the target exit into the lab angle interval subtended by the collimator at that point was then calculated. Finally, the momentum of each ray at the magnet system was calculated and the transmission of the magnet system for that ray determined from Fig. 10. A graph of $M(\Theta_{c.m.}, x) \cdot T(\Theta_{c.m.}) \sin\Theta_{c.m.}$ versus $\Theta_{c.m.}$, for the rays from the point x, was plotted. The area under the resulting curve was equal to

$$\int M(\Theta_{c.m.}, x) \cdot T(\Theta_{c.m.}) \sin\Theta_{c.m.} \, d\Theta_{c.m.} , \qquad (B\text{-}2)$$

for α-particles originating from point x. The above calculation was repeated for different positions along the incident deuteron beam line in the target and a graph of the expression (B-2) versus x obtained. The area under the curve, multiplied by the element of azimuthal angle

$\Delta\phi_{c.m.}$, subtended by the effective aperture of Q_1 at the center of the target, was then equal to the acceptance of the system for the particular nuclear reaction considered. The results for the various cases in this experiment are listed in Table V. The azimuthal angle $\Delta\phi_{c.m.}$, was determined from the expression

$$\Delta\phi_{c.m.} = \Delta\phi_{lab} = \frac{\ell v}{r \sin\theta_{lab}} = 0.29 \text{ radians}, \qquad \text{(B-3)}$$

where

ℓv = effective aperture of Q_1 in the vertical plane = 3.1 in.,

r = distance from Q_1 to the target center = 70.0 in., and

θ_{lab} = lab angle between secondary α-beam and primary deuteron beam = 8.7 deg.

C. Background Analysis

In this analysis we consider the following sources of background: (a) α-particle contamination of the incident deuteron beam, (b) α-particle production from deuteron-Al reactions in the target walls, and (c) sources of background that provide the same yield of α-particles into our system for D_2 and H_2 gas in the target.

The yield of α-particles obtained at each setting of the system can be described by an equation that includes the contributions from the above sources of background as well as the signal from the reaction being investigated. For purposes of clarity, we list the equations in Table VI. With reference to this table, then, the sig* π^0 is just the quantity sig π^0 degraded from 1060 MeV/c to 872 MeV/c at the target exit so that the two quantities are related by the expression

$$\frac{\text{sig}^*\ \pi^0}{\text{sig}\ \pi^0} = \frac{A^*_{\pi^0}\,(1 - X^*)}{A_{\pi^0}\,(1 - X)}, \qquad \text{(C-9)}$$

Table VI. Equations for background analysis

Setting: Magnet momentum $p(He^4)$ - MeV/c	Reaction	Target gas	Corresponding equation	
1060	$d+d \rightarrow He^4+\pi^0$	D_2	$sig\ \pi^0 + (\alpha\text{-}d)+(d\text{-}Al)_{D_2} + \chi(P_1) = 12.7\pm0.77$	(C-1)
1060	$d+d \rightarrow He^4+\pi^0$	H_2	$(\alpha\text{-}p)+(d\text{-}Al)_{H_2} + \chi(P_1) = 9.1\pm0.65$	(C-2)
1060	$d+d \rightarrow He^4+\gamma$	D_2	$sig\ \gamma + (\alpha\text{-}d)+(d\text{-}Al)_{D_2} + \chi(P_2) = 15.5\pm1.10$	(C-3)
1060	$d+d \rightarrow He^4+\gamma$	H_2	$(\alpha\text{-}p)+(d\text{-}Al)_{H_2} + \chi(P_2) = 10.5\pm0.82$	(C-4)
872	$d+d \rightarrow He^4+\pi^0$	D_2	$sig^*\pi^0 + [(\alpha\text{-}d)+(d\text{-}Al)_{D_2} + \chi(P_1)]\ N = 8.1\pm1.07$	(C-5)
872	$d+d \rightarrow He^4+\pi^0$	H_2	$[(\alpha\text{-}p)+(d\text{-}Al)_{D_2} + \chi(P_1)]\ N = 4.4\pm0.59$	(C-6)
872	$d+d \rightarrow He^4+\gamma$	D_2	$sig^*\gamma + [(\alpha\text{-}d)+(d\text{-}Al)_{D_2}]\ N + \chi(P_3) = 9.3\pm0.82$	(C-7)
872	$d+d \rightarrow He^4+\gamma$	H_2	$[(\alpha\text{-}p)+(d\text{-}Al)_{H_2}]\ N + \chi(P_3) = 5.3\pm0.53$	(C-8)

where $sig\ \pi^0$ = yield from the π^0 reaction.

$sig^*\pi^0$ = yield from the π^0 reaction under the experimental conditions associated with Eq. (C-5)

$sig\ \gamma$ = yield from the γ reaction with the system set for $\Theta_{c.m.} = 65$ deg,

$sig^*\gamma$ = yield from the γ reaction with the system set for $\Theta_{c.m.} = 135$ deg,

$(\alpha\text{-}d)$ = yield from alpha contamination of the incident beam scattering in the D_2,

$(\alpha\text{-}p)$ = yield from alpha contamination of the incident beam scattering in the H_2,

$(d\text{-}Al)_{D_2}$ = yield from deuteron-Al interactions in the target walls, for D_2 target.

$(d\text{-}Al)_{H_2}$ = yield from deuteron-Al interactions in the target walls, for H_2 target.

$\chi(P)$ = yield from momentum-dependent sources of background whose effects are the same for D_2 and H_2 targets.

N = background normalization factor to account for the fact that the yield from various sources of background is a function of the magnet system settings. As used above, this factor normalizes the particular background yield obtained at magnet momentum of 872 MeV/c to that obtained at 1060 MeV/c.

For the above expressions, the yield is taken to mean the α-particle yield per 10^{13} incident deuterons.

where $A^{*}_{\pi^0}$, A_{π^0} = acceptance of the system for the π^0 reaction for magnet momenta, $P(He^4)$, of 872 MeV/c and 1060 MeV/c, respectively (Table V), and

X*, X = fraction of the alpha signal that did not pass through the entire counter telescope owing to multiple scattering in T_1 and T_2 counters, for magnet momenta of 872 MeV/c and 1060 MeV/c, respectively: X* = 10% and X = 3%.

With the assumption that the angular distribution of the γ reaction is of the form $\sin^2\Theta_{c.m.} \cos^2\Theta_{c.m.}$,[5] the relation between sig*γ and sig γ can be expressed as

$$\frac{\text{sig}^*\gamma}{\text{sig}\ \gamma} = \frac{A^*_\gamma (1 - X^*) \sin^2 135^\circ \cos^2 135^\circ}{A_\gamma (1 - X) \sin^2 65^\circ \cos^2 65^\circ} , \qquad \text{(C-10)}$$

where A^*_γ, A_γ = acceptance of the system for the γ reaction with the system set for $\Theta_{c.m.}$ = 135 deg and 65 deg, respectively (Table V), and

X*, X = same as in expression (C-9).

From the measurements with an alpha beam from the cyclotron incident on the D_2 and H_2 targets, we have

$$(\alpha\text{-d}) = 1.48\ (\alpha\text{-p}) . \qquad \text{(C-11)}$$

Additionally, the data in Table II indicate

$$(\text{d-Al})_{D_2} = 1.42\ (\text{d-Al})_{H_2} . \qquad \text{(C-12)}$$

Thus, we have 12 equations and 12 unknowns; solving these for sig π^0 and sig γ, we obtain

$$\text{sig } \pi^0 = -12.5 \pm 11.5 \text{ alpha counts per } 10^{13} \text{ incident deuterons,} \tag{C-13}$$

and

$$\text{sig } \gamma = 3.8 \pm 2.8 \text{ alpha counts per } 10^{13} \text{ incident deuterons.} \tag{C-14}$$

The differential cross sections corresponding to these counting rates are calculated from Eq. (9). The results appear in expressions (16) and (17) in the text.

REFERENCES

1. A summary of the more recent experiments is given by B. Pontecorvo, in Proceedings of the 1959 International Conference on High-Energy Physics at Kiev, 1959.
2. A. V. Crewe, E. Yarwin, B. Ledley, E. Lillethim, R. March, and S. Marcowitz, Phys. Rev. Letters 2, 269 (1959).
3. K. R. Greider, Phys. Rev. 122, 1919 (1961).
4. Norman E. Booth, Owen Chamberlain, and Ernest H. Rogers, Search for a Neutral Meson of Zero I Spin, Nuovo cimento 19, 853 (1961).
5. Yu K. Akimov, O. V. Savchenko, and L. M. Soroko, in Proceedings of the 1960 International Conference on High-Energy Physics at Rochester (Interscience Publishers, Inc., New York); the same authors repeated the experiment after ours was completed and found $\sigma_t < 1.1 \times 10^{-32}$ cm^2, see Soviet Physics JETP 14, 512 (1962).
6. E. R. Gaerttner and M. L. Yeater, Phys. Rev. 83, 146 (1951).
7. A. Gorbunov and V. Spividonov, Soviet Physics JETP 6, 16 (1958).
8. Ernest H. Rogers (Lawrence Radiation Laboratory) private communication.
9. Rudolf R. Larsen, Experiments on Neutron-Proton Scattering and Determination of the Pion-Nucleon Coupling Constant, (Thesis) UCRL-9292, July 1960.
10. K. L. Brown, Rev. Sci. Instr. 27, 956 (1956).
11. W. K. H. Panofsky and J. A. McIntyre, Rev. Sci. Instr. 25, 287 (1954).
12. Samuel Penner, Calculations of Properties of Magnetic Deflection Systems, National Bureau of Standards Internal Report, 1958 (unpublished).

13. Thomas J. Devlin, Optik: An IBM 709 Computer Program for the Optics of High-Energy Particle Beams, UCRL-9727, Sept. 1961.

14. James D. Young, Optic Analog for a Symmetric Quadrupole, UCRL-9054, Jan. 1960.

15. William M. Cross, Rev. Sci. Instr. 22, 717 (1951).

16. Ernest D. Courant, M. Stanley Livingston, and Hartland S. Snyder, Phys. Rev. 88, 1190 (1952).

17. Edwin M. McMillan, Notes on Quadrupole Focusing, UCRL-3333, Feb. 1956.

18. Lawrence Radiation Laboratory Counting Handbook, UCRL-3307 Rev., Jan. 1959.

19. William A. Wenzel, Millimicrosecond Coincidence Circuit for High-Speed Counting, UCRL-8000, Oct. 1957.

20. T. J. Gooding and H. G. Pugh, Nuclear Instr. & Methods 7, 189 (1960).

21. L. Shechter, W. E. Crandall, G. P. Millburn, D. A. Hicks, and A. V. Shelton, Phys. Rev. 90, 633 (1953).

22. G. P. Millburn, W. Birnbaum, W. E. Crandall, and L. Shechter, Phys. Rev. 95, 1268 (1954).

23. B. H. Flowers and F. Mandl, Proc. Roy. Soc. (London) 206, 131 (1951).

24. A. Baldin, Nuovo cimento 8, 569 (1958).

25. O. Chamberlain, E. Segrè, and C. Wiegand, Phys. Rev. 83, 923 (1951).

26. W. A. Aron, B. G. Hoffman, and F. C. Williams, Range-Energy Curves UCRL-121 (2nd Rev.) October 1949. (AECU-666).

27. Bruno Rossi, High-Energy Particles, Sec. 2.17 (Prentice-Hall, Inc., New York, 1952). To account for the energy loss of the α-particles in the D_2, the mean α-particle momentum in the D_2 was used in the calculation of the lateral displacement.

28. Hans A. Bethe and Julius Ashkin, Passage of Radiation through Matter, in Experimental Nuclear Physics, E. Segrè, Ed. (John Wiley and Sons, Inc., New York, 1953), Vol. I, p. 166. Formula (78) is the one used for the mean-square multiple-scattering angle and formula (76) is used for the calculation of probability of scattering into a definite angular interval in the horizontal or vertical plane.